Cell Reports

Article

KAT2B Is Required for Pancreatic Beta Cell Adaptation to Metabolic Stress by Controlling the Unfolded Protein Response

Graphical Abstract

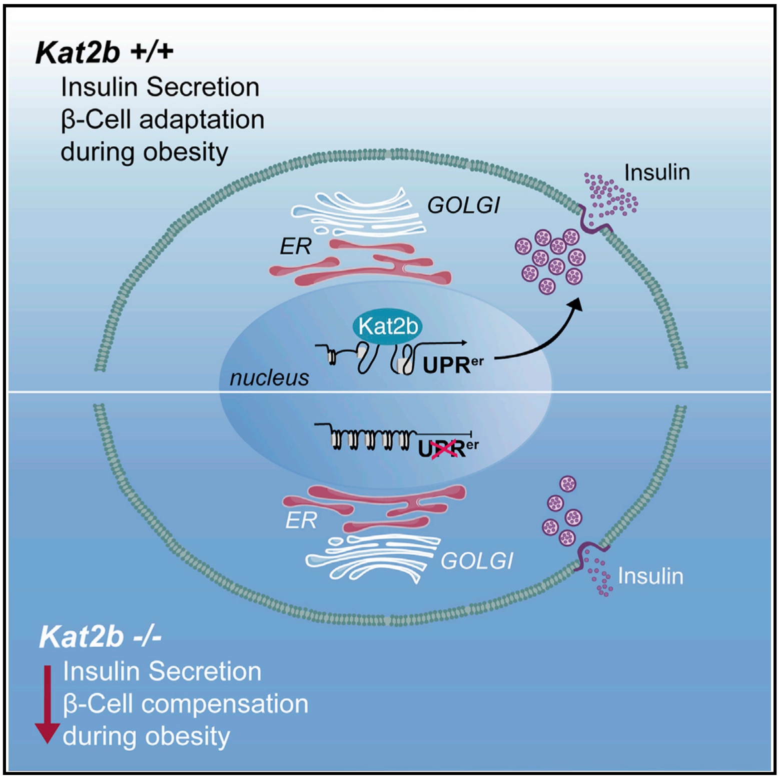

Highlights

- The expression of UPR markers is altered in diabetic islets
- Loss of *Kat2b* contributes to defective insulin secretion and β cell compensation
- KAT2B regulates an UPR gene program in pancreatic β cells
- KAT2B expression is reduced in mouse and human diabetic β cells

Authors

Nabil Rabhi, Pierre-Damien Denechaud, Xavier Gromada, ..., Lluis Fajas, Philippe Froguel, Jean-Sébastien Annicotte

Correspondence

p.froguel@imperial.ac.uk (P.F.), jean-sebastien.annicotte@inserm.fr (J.-S.A.)

In Brief

Rabhi et al. reveal a role for Kat2b in the control of insulin secretion and pancreatic β cell adaptation to metabolic stress through cell-autonomous regulation of the unfolded protein response (UPR). These data collected demonstrate that Kat2b expression is decreased in diabetic islets and suggest molecular links among KAT2B, the UPR, and diabetes.

Accession Numbers

GSE78860

Rabhi et al., 2016, Cell Reports *15*, 1051–1061
May 3, 2016 ©2016 The Authors
http://dx.doi.org/10.1016/j.celrep.2016.03.079

OPEN ACCESS
CellPress

KAT2B Is Required for Pancreatic Beta Cell Adaptation to Metabolic Stress by Controlling the Unfolded Protein Response

Nabil Rabhi,[1,2,3] Pierre-Damien Denechaud,[4] Xavier Gromada,[1,2,3] Sarah Anissa Hannou,[1,2,3] Hongbo Zhang,[5] Talha Rashid,[1,2,3] Elisabet Salas,[1,2,3] Emmanuelle Durand,[1,2,3] Olivier Sand,[1,2,3] Amélie Bonnefond,[1,2,3] Loic Yengo,[1,2,3] Carine Chavey,[6] Caroline Bonner,[7] Julie Kerr-Conte,[7] Amar Abderrahmani,[1,2,3] Johan Auwerx,[5] Lluis Fajas,[4] Philippe Froguel,[1,2,3,8,*] and Jean-Sébastien Annicotte[1,2,3,*]
[1]University Lille, UMR 8199 - EGID, 59000 Lille, France
[2]CNRS, UMR 8199, 59000 Lille, France
[3]Institut Pasteur de Lille, 59000 Lille, France
[4]Department of Physiology, University of Lausanne, 1005 Lausanne, Switzerland
[5]Laboratory for Integrative and Systems Physiology, Swiss Federal Institute of Technology, 1015 Lausanne, Switzerland
[6]Institut de Génétique Moléculaire de Montpellier, CNRS, UMR 5535, 34298 Montpellier, France
[7]University Lille, INSERM, CHU Lille, U1190 - EGID, 59000 Lille, France
[8]Departments of Genomics and Common Disease, School of Public Health, Imperial College London, Hammersmith Hospital, London W12 0NN, UK
*Correspondence: p.froguel@imperial.ac.uk (P.F.), jean-sebastien.annicotte@inserm.fr (J.-S.A.)
http://dx.doi.org/10.1016/j.celrep.2016.03.079

SUMMARY

The endoplasmic reticulum (ER) unfolded protein response (UPR^{er}) pathway plays an important role in helping pancreatic β cells to adapt their cellular responses to environmental cues and metabolic stress. Although altered UPR^{er} gene expression appears in rodent and human type 2 diabetic (T2D) islets, the underlying molecular mechanisms remain unknown. We show here that germline and β cell-specific disruption of the lysine acetyltransferase 2B (*Kat2b*) gene in mice leads to impaired insulin secretion and glucose intolerance. Genome-wide analysis of Kat2b-regulated genes and functional assays reveal a critical role for Kat2b in maintaining UPR^{er} gene expression and subsequent β cell function. Importantly, Kat2b expression is decreased in mouse and human diabetic β cells and correlates with UPR^{er} gene expression in normal human islets. In conclusion, Kat2b is a crucial transcriptional regulator for adaptive β cell function during metabolic stress by controlling UPR^{er} and represents a promising target for T2D prevention and treatment.

INTRODUCTION

The endoplasmic reticulum (ER) is a crucial organelle necessary to maintain protein folding and secretory capacity. Defective ER function or prolonged ER stress impairs glucose homeostasis and is associated with the development of peripheral insulin resistance and impaired β cell function, two major contributors to the pathogenesis of diabetes (Walter and Ron, 2011; Wang and Kaufman, 2012). Several lines of genetic evidence suggest that the transition between an obese, insulin-resistant state to type 2 diabetes (T2D) is triggered by β cell failure, due to both a partial loss of β cell mass and an impaired β cell function (Muoio and Newgard, 2008). Interestingly, obese patients maintaining β cell compensation are protected from T2D, suggesting that the mechanisms controlling this particular stage of diabetes progression is crucial for the evolution to diabetes (Weir and Bonner-Weir, 2004).

Pancreatic β cells adapt their secretory capacity to metabolic challenges by activating the ER unfolded protein response (UPR^{er}), particularly during diet-induced obesity (Eizirik and Cnop, 2010). The UPR^{er} orchestrates complex signaling pathways in specialized secretory cells undergoing ER stress (Hetz, 2012). Typically, the UPR^{er} is composed of three transmembrane ER stress sensors, ATF6, IRE1 and PERK, that transduce signaling pathways and, finally, modify the expression of key genes leading to adaptive responses and recovery from ER stress (Back and Kaufman, 2012). A growing body of evidence suggests that alteration in the expression of UPR^{er} genes may lead to β cell failure and contribute to diabetes development (Cnop et al., 2012; Rabhi et al., 2014). Recent studies in mouse and human diabetic islets implicate altered expression of these markers (Chan et al., 2013; Engin et al., 2014; Kennedy et al., 2010; Laybutt et al., 2007). However, the upstream regulators responsible for the modulation of UPR^{er} gene expression are currently unknown.

Gene expression relies on the epigenetic status of histones, transcription factors, and their coregulators, allowing cell adaptation to metabolic change (Kelly and Scarpulla, 2004; Mouchiroud et al., 2014). Adapted responses to different environmental metabolic cues are controlled through the balance between acetylation and deacetylation of specific histone marks and transcription factors (Menzies et al., 2016; Mihaylova and Shaw, 2013; Zhao et al., 2010). This process involves the antagonistic activity of the chromatin-modifying enzymes lysine/histone deacetylase (KDAC) and lysine/histone acetyl transferase (KAT). Accumulating evidence suggests important roles for KDACs in the control of glucose homeostasis (Mihaylova and Shaw, 2013), notably by regulating endocrine pancreatic development (Haumaitre et al., 2008; Lenoir et al., 2011) and β cell function and survival (Lundh et al., 2012; Plaisance et al., 2014). So far, little is known about the metabolic role of KAT, in particular KAT2B. In this study, we investigated the effect of germline and β cell-specific *Kat2b* deficiency on glucose homeostasis and insulin secretion. We find that loss of *Kat2b* induces defects in insulin secretion and glucose intolerance. We further establish direct links among Kat2b, UPR^{er} gene expression, and insulin secretion. We also demonstrate that *KAT2B* expression is defective in T2D islets, providing an unsuspected mechanistic link among KAT2B, UPR^{er} signaling, the ER stress response, and β cell function during metabolic stress.

RESULTS AND DISCUSSION

Germline and β Cell-Specific *Kat2b* Deficiency Impairs Glucose Tolerance and Insulin Secretion in Mice

To elucidate the role of KAT2B in glucose homeostasis, we first investigated the metabolic phenotype of *Kat2b*-deficient mice (*Kat2b* −/−) (Maurice et al., 2008; Yamauchi et al., 2000). Body weight and size of *Kat2b* −/− mice under a chow diet was reduced when compared to controls (Figures S1A and S1B). The reduced body size was not caused by changes in Igf-1 levels, as liver *Igf-1* mRNA levels and serum Igf-1 concentrations were unchanged (Figures S1C and S1D). *Kat2b*-deficient mice displayed a slight elevation of blood glucose values that was associated with a decrease in plasma insulin levels (Figures 1A and 1B). Insulin sensitivity was similar between both genotypes (Figure 1C), indicating that hyperglycemia in *Kat2b* −/− mice may result from insulinopenia. *Kat2b* −/− mice tended to respond to intraperitoneal glucose tolerance tests (ipGTTs; Figures 1D and 1E; $p = 0.06$), despite decreased insulin secretion in response to glucose (Figure 1F). In contrast to mice fed a regular diet, *Kat2b* −/− mice fed a high-fat diet (HFD) developed hyperglycemia (Figure 1G), insulinopenia (Figure 1H), and impaired glucose tolerance (Figures 1I and 1J). Impaired glucose homeostasis was correlated with a significant reduction of glucose-stimulated insulin levels (Figure 1K), despite moderate weight gain (Figure S1E; $p < 0.01$). Insulin sensitivity was similar between *Kat2b*+/+ and *Kat2b* −/− mice fed an HFD (Figure 1L).

We next found that KAT2B protein co-localizes with insulin in healthy rodent islets (Figures 1M, S1F, and S1G). We then investigated glucose-stimulated insulin secretion (GSIS) in isolated pancreatic islets from *Kat2b* −/− mice. Although *Kat2b* deletion did not affect the total insulin content (Figure S1H), it reduced GSIS by 56% (Figure 1N). Reduction of GSIS was further confirmed in Min6 cells in which *Kat2b* expression was silenced using interfering RNAs (Figures S1I and S1J). Islet histology (Figure S1K) and cell number and surface area (Figure 1O) were similar in chow-fed *Kat2b* −/− mice. However, islet size of *Kat2b* −/− mice fed an HFD was significantly reduced when compared to controls (Figure 1O; $p < 0.001$; Figure S1K). Reduction of islet size was correlated with an increased proportion of small islets (Figure S1L). The number of α and β cells per islet and circulating glucagon levels were similar for both diets (Figures S1M–S1P). With an HFD only, a significant decrease in β cell area was observed in *Kat2b* −/− pancreata compared to controls (Figure 1P; $p < 0.001$; Figure S1M), suggesting that Kat2b is required for β cell compensation in obesity and associated insulin resistance.

To further demonstrate the cell-autonomous function of Kat2b on insulin secretion, we generated β cell-specific *Kat2b* knockout mice by crossing $Kat2b^{Lox/Lox}$ with RIP-Cre mice (Herrera, 2000) (hereafter referred as $Kat2b^{\beta-/-}$; Figure S2A). *Kat2b* gene expression analysis on isolated islets demonstrated an efficient recombination upon β cell-specific Cre recombinase expression at the *Kat2b* locus (Figure 2A), but not in other metabolic organs including hypothalamus, liver, or adipose tissues (Figure S2B). Body weight and fasting glucose levels were similar among all genotypes (Figures 2B and 2C, respectively). As observed in the germline *Kat2b* −/− mice, the β cell-specific deletion of *Kat2b* resulted in glucose intolerance (Figures 2D and 2E). The $Kat2b^{\beta-/-}$ mice had blunted insulin release 30 min after intraperitoneal glucose administration (Figure 2F), whereas their systemic insulin sensitivity was preserved (Figure 2G). Challenging $Kat2b^{\beta-/-}$ mice with an HFD resulted in moderate body weight gain (Figure 2H) and normal fasting glucose levels (Figure 2I). However, $Kat2b^{\beta-/-}$ mice fed an HFD were glucose intolerant (Figures 2J and 2K), with defective insulin secretion after intraperitoneal glucose administration (Figure 2L), but remained sensitive to insulin (Figure 2M). Although we cannot rule out off-target effects during our small interfering RNA (siRNA) experiments, these results suggest that Kat2b modulates insulin secretion in a cell-autonomous manner and may contribute to β cell compensation during metabolic stress.

Kat2b Directly Regulates an UPR^{er} Gene Program Necessary for Proper Insulin Secretion

Kat2b directly regulates insulin gene expression in response to glucose through the acetylation of histone H4 (Sampley and Ozcan, 2012). However, isolated islets from *Kat2b* +/+ *and* −/− mice showed no difference in mRNA levels of key genes involved in insulin synthesis (*Ins1*, *Ins2*, *Pdx1*, and *Mafa*), maturation (*Pcsk1*, *Pcsk2*, and *Cpe*), or secretion (*Slc30a8*, *Kcnj11*, *Abcc8*, and *ChgA*; Figure S3A). As Kat2b is a transcriptional coregulator, we performed chromatin immunoprecipitation sequencing (ChIP-seq) in murine isolated islets and showed that DNA motifs present in regions bound by Kat2b were those recognized by several transcription factors, including Pax4, Creb1, Atf4, Atf6, Ddit3 (Chop), and Xbp1 (Table S1). Recent evidence demonstrated that altered expression of genes involved in UPR^{er} impairs insulin secretion and β cell function (Back and Kaufman, 2012). We hypothesized that this pathway may be controlled by Kat2b, and we focused our ChIP-seq analysis on the ER. Gene Ontology (GO) analysis revealed an enrichment of sequences bound by Kat2b involved in different cellular and biological regulations, including the cellular response to a stimulus, the metabolic process, or response to stress (Table S2). GO analysis revealed that many genes controlling ER functions ($p = 6.4 \times 10^{-13}$), the ER stress response ($p = 0.0027$), and UPR^{er} signaling ($p = 0.039$; Table S2) are Kat2b targets. Consistently, Kat2b

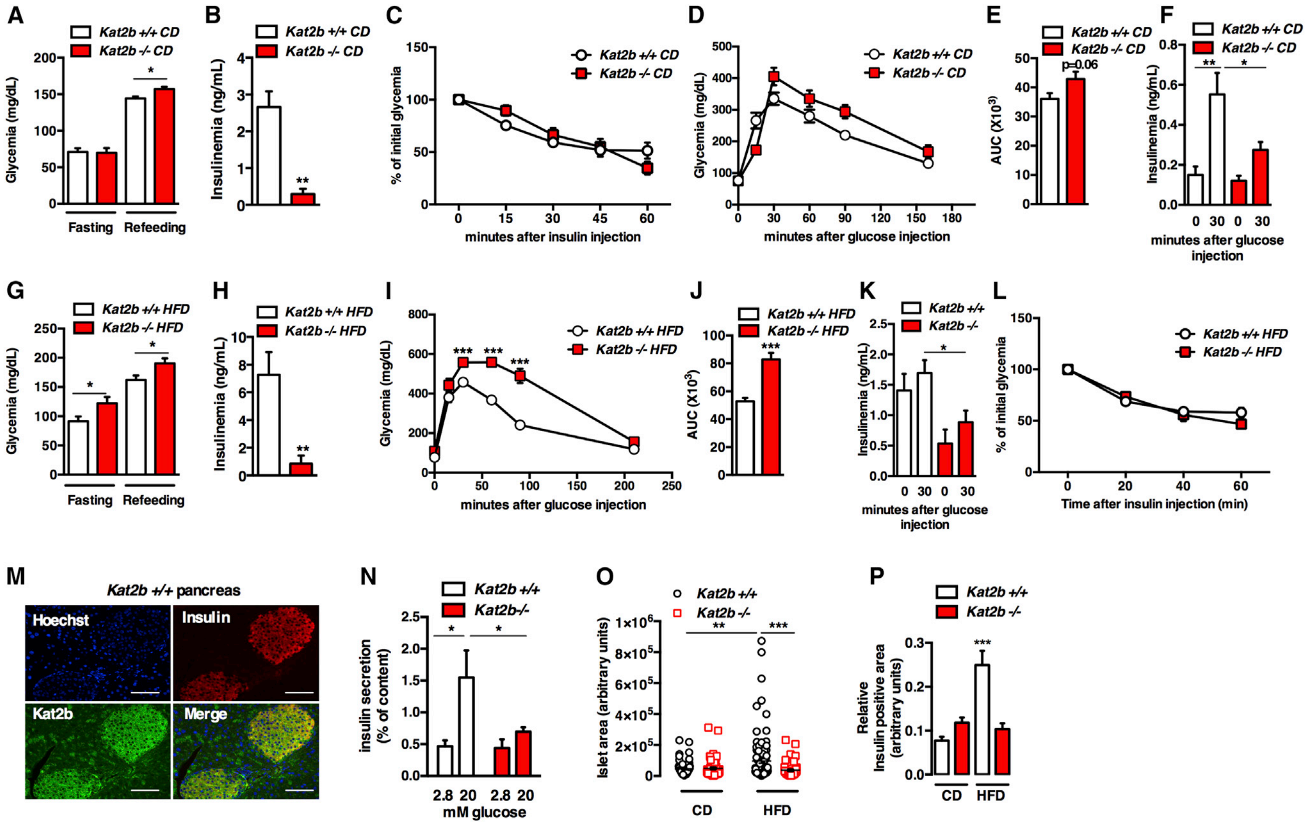

Figure 1. Loss of *Kat2b* in Mice Causes Glucose Intolerance and Insulinopenia

(A and B) 16-hr fasting and refed blood glucose levels (A) and refed serum insulin levels (B) in 12-week-old control (*Ka2b* +/+) and mutant (*Kat2b* −/−) mice (n = 4–7).

(C) blood glucose levels during intraperitoneal insulin tolerance test (ipITT) in mice fed normal chow (n = 6).

(D–F) ipGTT (D), area under the curve (AUC) of ipGTT (E), and serum insulin levels at the indicated times after intraperitoneal injection of glucose (F) (n = 6).

(G and H) 16-hr fasting and refed blood glucose levels (G) and refed serum insulin levels (H) in *Kat2b* +/+ *and* −/− mice fed an HFD for 13 weeks (n = 7−10).

(I–L) Blood glucose levels during ipGTT (I), AUC of ipGTT with an HFD (J), serum insulin levels at the indicated times after intraperitoneal injection of glucose (K), and blood glucose levels during ipITT in mice fed an HFD (L) (n = 7–10).

(M) Immunofluorescence analysis of pancreatic sections showing co-expression of Kat2b (green) and insulin (red) in mouse pancreatic islets. Nuclei are stained with Hoechst reagent (scale bar, 100 μm).

(N) Insulin secretion from islets isolated from *Kat2b* +/+ (gray bars) and −/− (red bars) mice in the presence of 2.8 mM and 20 mM glucose. Results were normalized to total insulin content (n = 3).

(O) Quantification of islet area in *Kat2b* +/+ and −/− pancreata of mice fed normal chow or an HFD (n = 5 animals per condition). All individual values are plotted on the graph.

(P) Quantification of relative insulin-positive area from pancreatic sections of *Kat2b* +/+ and −/− mice fed chow and an HFD.

All values are expressed as means ± SEM; *p < 0.05, **p < 0.01, and ***p < 0.001.

occupies the promoters of several genes controlling UPR^{er} activity, including *Xbp1*, *Hspa5* (*BiP*), *Atf4*, and *Atf6* (Table S3; Figure S3B).

As ER homeostasis is critical for maintaining β cell function (Fonseca et al., 2011), we investigated how impaired UPR^{er} regulation in *Kat2b* −/− islets led to defective insulin secretion. It was previously shown that treatment with chemical chaperones, such as taurine-conjugated ursodeoxycholic acid (TUDCA) and 4-phenyl butyric acid (4-PBA), alleviates ER stress and prevents glucose-induced β cell dysfunction (Tang et al., 2012). Treatment with both TUDCA and 4-PBA partially rescued GSIS in isolated pancreatic *Kat2b* −/− islets (Figure 3A), suggesting that UPR dysfunction could be responsible for insulin secretion defects. In *Kat2b*-silenced Min6 cells, treatment with both molecules also restored GSIS (Figure S3C). In accordance with ChIP-seq data, the expression of UPR^{er} genes was decreased in isolated *Kat2b* −/− islets (Figure 3B). This effect was further observed in *Kat2b* −/− mice fed an HFD (Figure 3C), concomitantly with associated decreased expression of key β cell genes such as *Mafa*, *Ins2*, and *Cpe* (Figure S3D). Decreased expression of several UPR^{er} genes was confirmed in *Kat2b*$^{\beta-/-}$ islets (Figure 3D). *Kat2b* silencing in Min6 cells further showed UPR^{er} pathway impairment (Figure S3E) and decreased expression of β cell genes (Figure S3F). Therefore, these findings suggest that Kat2b is an upstream transcriptional regulator of UPR^{er} markers in murine pancreatic islets and Min6 insulinoma cells.

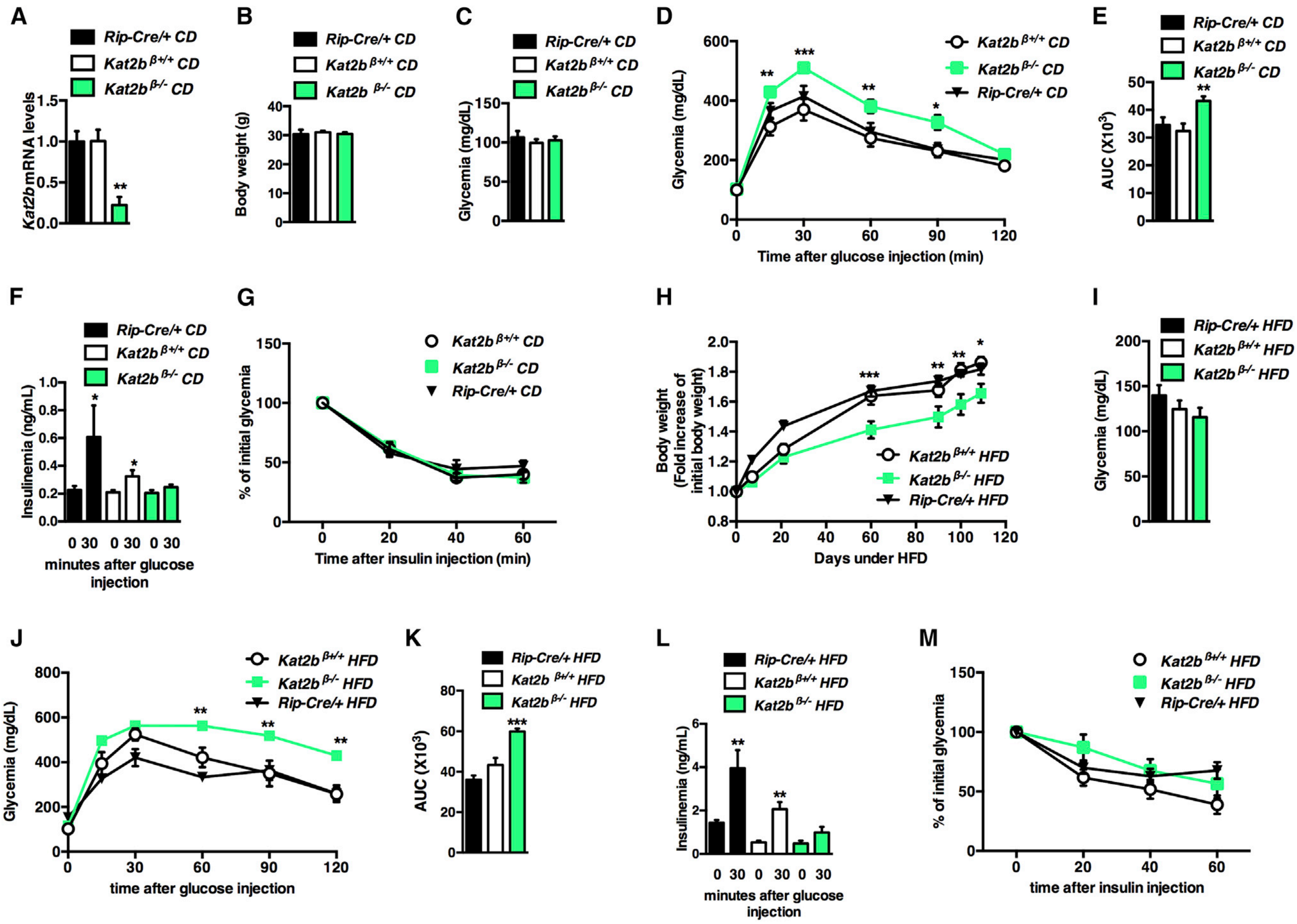

Figure 2. Impaired Glucose Tolerance in Mice with a β Cell-Specific Knockout of *Kat2b*

(A) *Kat2b* mRNA levels in islets isolated from control (*Rip-Cre*/+ and *Kat2b*$^{β+/+}$) and β cell-specific mutant (*Kat2b*$^{β-/-}$) mice.

(B and C) Body weight (B) (n = 9–14) and 16-hr fasting blood glucose levels (C) (n = 11) in *Rip-Cre*/+, *Kat2b*$^{β+/+}$, and *Kat2b*$^{β-/-}$ mice fed normal chow.

(D–F) ipGTT measuring the levels of glucose (D), the corresponding AUC (E) and insulin (F) at the indicated times after intraperitoneal injection of glucose in 5-month-old *Rip-Cre*/+ (black triangles and bars, n = 11), *Kat2b*$^{β+/+}$ (white circles and bars, n = 11), and *Kat2b*$^{β-/-}$ (green squares and bars, n = 11).

(G) ipITT measuring levels of glucose at the indicated times after intraperitoneal injection of insulin in mice fed normal chow (n = 11).

(H) Body weight gain under HFD feeding of *Rip-Cre*/+ (n = 8), *Kat2b*$^{β+/+}$ (n = 6), and *Kat2b*$^{β-/-}$ (n = 10).

(I) 16 hr fasting blood glucose levels in *Rip-Cre*/+ (n = 4), *Kat2b*$^{β+/+}$ (n = 10), and *Kat2b*$^{β-/-}$ (n = 11) mice fed an HFD for 16 weeks.

(J–L) ipGTT measuring the levels of glucose (J), the corresponding AUC (K), and serum insulin (L) at the indicated times after intraperitoneal injection of glucose in *Rip-Cre*/+ (black triangles and bars, n = 11), *Kat2b*$^{β+/+}$ (white circles and bars, n = 11), and *Kat2b*$^{β-/-}$ (green squares and bars, n = 11) mice fed an HFD for 16 weeks.

(M) ipITT measuring the levels of glucose at the indicated times after intraperitoneal injection of insulin in mice fed an HFD (n = 6–11).

All values are expressed as mean ± SEM. *p < 0.05, **p < 0.01, and ***p < 0.001.

Germline or β cell-specific *Atf6*-deficient (*Atf6*$^{β-/-}$) mice have decreased insulin secretion (Engin et al., 2014; Usui et al., 2012). The striking similarity between the *Kat2b* −/− mice and *Atf6*-deficient mice prompted us to focus on the regulation of the *Atf6* gene by Kat2b. In agreement with our ChIP-seq and qPCR data, luciferase-based reporter studies confirmed that Kat2b potentiates the promoter activity of the *Atf6* gene construct in Min6 cells (Figure 4A). This transcriptional effect relied on Kat2b acetyltransferase activity. A Kat2b construct deleted of its HAT domain was unable to stimulate the luciferase gene (Figure 4A). Importantly, rescue of *Atf6* expression in *Kat2b* −/− islets (Figures 4B and S4A) and in *Kat2b*-silenced Min6 cells (Figures 4C and S4B) restored glucose-stimulated insulin secretion in these cells, demonstrating that *Atf6* mediated the observed effects of Kat2b on insulin secretion. To further evaluate the contribution of Kat2b to the ER stress response, we treated Min6 cells with the ER stress inducer thapsigargin (TG). This treatment did not modulate *Kat2b* mRNA levels (Figure 4D), but it rapidly increased Kat2b protein levels (Figures 4E and 4F). The rise of Kat2b abundance by TG was confirmed at lower doses (Figure S4C) and in cells exposed to the lipotoxic agent palmitate (Figure S4D). Interestingly, we identified a potential upstream open reading frame (uORF) within the *Kat2b* gene that may contribute to this

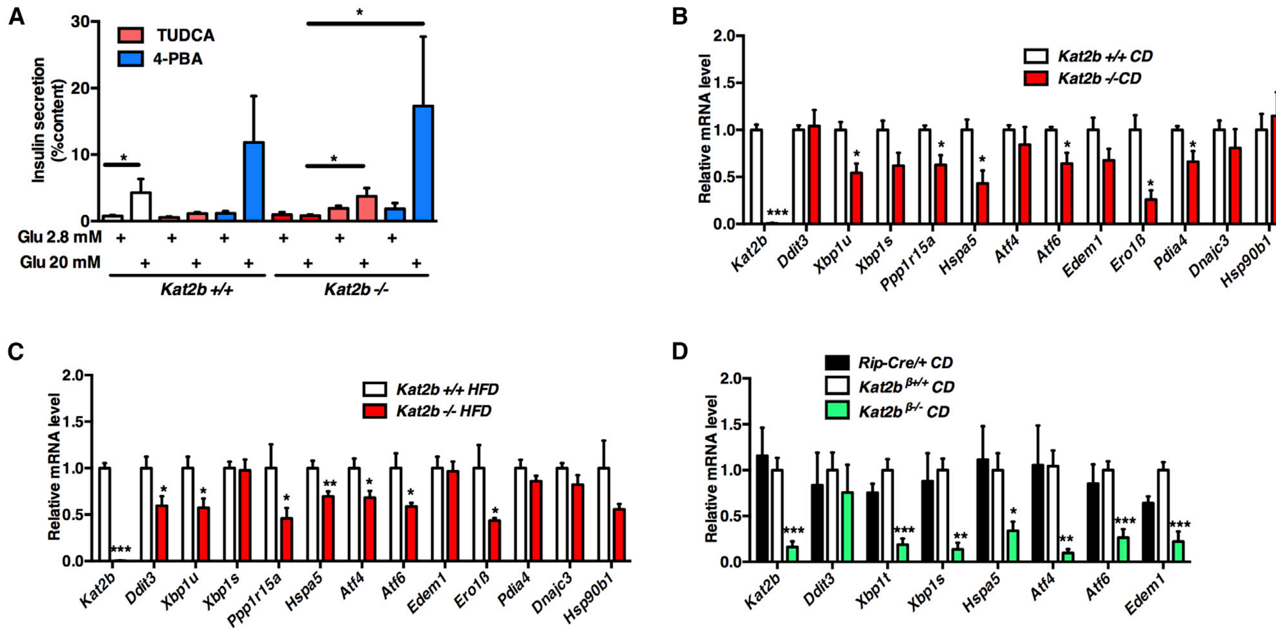

Figure 3. Modulation of UPR^{er} Signaling in Murine *Kat2b* −/− β Cells Is Required for Insulin Secretion

(A) Effects of TUDCA and 4-PBA treatments on glucose-stimulated insulin secretion from *Kat2b* +/+ and −/− isolated islets (n = 3).

(B and C) mRNA levels of UPR^{er} genes in islets isolated from *Kat2b* +/+ and −/− mice fed chow (B) or an HFD (C) (n = 4–5).

(D) mRNA levels of UPR^{er} genes in islets isolated from *Rip-Cre/+*, *Kat2b*$^{\beta+/+}$, and *Kat2b*$^{\beta-/-}$ mice fed chow (n = 3).

Data are shown as mean ± SEM. *p < 0.05, **p < 0.01, and ***p < 0.001.

regulation (data not shown). In contrast to *Kat2b*, TG increased *Atf6* mRNA levels (Figure 4G). This induction was lowered upon *Kat2b* silencing, suggesting that Kat2b may contribute to *Atf6* regulation under stress conditions (Figure 4G). ChIP-qPCR in Min6 cells confirmed Kat2b binding on the *Atf6* promoter (Figure 4H). The regulation of the *Atf6* promoter by Kat2b was independent of histone H3 acetylation, since no modulation of the H3ac, H3K9ac, or H3K14ac epigenetic marks was observed upon *Kat2b* silencing in Min6 cells (Figure S4E). The *Pdx1* promoter was, however, modulated by Kat2b-dependent acetylation of histone H3 (Figure S4E). This suggests that the regulation of *Atf6* promoter activity may operate through the acetylation of non-histone proteins. Moreover, recruitment of Kat2b on the *Atf6* promoter was increased in the presence of TG (Figure 4H). To further study the contribution of Kat2b in UPR^{er} signaling, activation of several key UPR^{er} proteins was monitored upon reduction of *Kat2b* levels. Silencing of *Kat2b* decreased the amount of total PERK, phosphorylated PERK, Hspa5, phosphorylated IRE1a, and its target, spliced Xbp1 and Atf6, in response to TG treatment (Figure 4I). Altogether, these data suggest that Kat2b is a permissive transcriptional co-activator controlling several branches of the UPR^{er} pathway under both basal and stress conditions. Our results also emphasize that Kat2b mostly affects the Atf6 branch of the UPR^{er}. The regulation of the *Kat2b* uORF by the PERK-eIF2a arm of the UPR is currently unknown but might represent a mechanistic link between ER-stress-dependent UPR^{er} activation and the regulation of UPR^{er} target genes targeted by Kat2b.

Decreased Kat2b Expression in Rodent and Human T2D Islets

We then quantified Kat2b expression in rodents and human diabetic islets. Kat2b expression was significantly reduced in 20-week-old *db/db* pancreatic islets compared to non-diabetic *db/+* mice (Figures 5A and 5B). Immunofluorescence assays on formalin-fixed human pancreatic sections showed that insulin-producing β cells and non-β cells expressed KAT2B (Figure 5C). Islet transcriptomics analysis in T2D subjects from two independent datasets demonstrated a significant decrease of *KAT2B* mRNA levels compared to normal glycemic controls (GEO: GSE20966; Marselli et al., 2010; and GEO: GSE38642; Taneera et al., 2012; Figures 5D and 5E, respectively). Moreover, *KAT2B* expression in human islets was inversely correlated with the long-term glucose control marker glycated hemoglobin A1c (HbA1c; Figure 5F). By analyzing fresh human islets isolated from four T2D donors and four normoglycemic subjects (see Table S4 for donor information), we confirmed that *KAT2B* expression was decreased in T2D (Figure 5G). Some UPR^{er} pathways are defective in human T2D islets; Engin et al., 2014; Kennedy et al., 2010). In this respect, *KAT2B* expression, *ABCC8*, *SLC30A8*, *CPE*, *PDX1*, and UPR^{er} genes *DDIT3* (*CHOP*), *HERPUD2*, *HSP90B1* (*GRP94*), *EDEM1*, and *DNAJC3 (p58IPK)* were concomitantly decreased in T2D islets (Figure 5H). In human islets, *KAT2B* and the expression of genes controlling UPR^{er} and β cell function were positively correlated (Figure 5I). Moreover, *KAT2B*, UPR^{er} and β cell function genes are part of the same gene cluster (Figure 5J). Silencing of *KAT2B* expression in healthy human islets

OPEN
ACCESS
CellPress

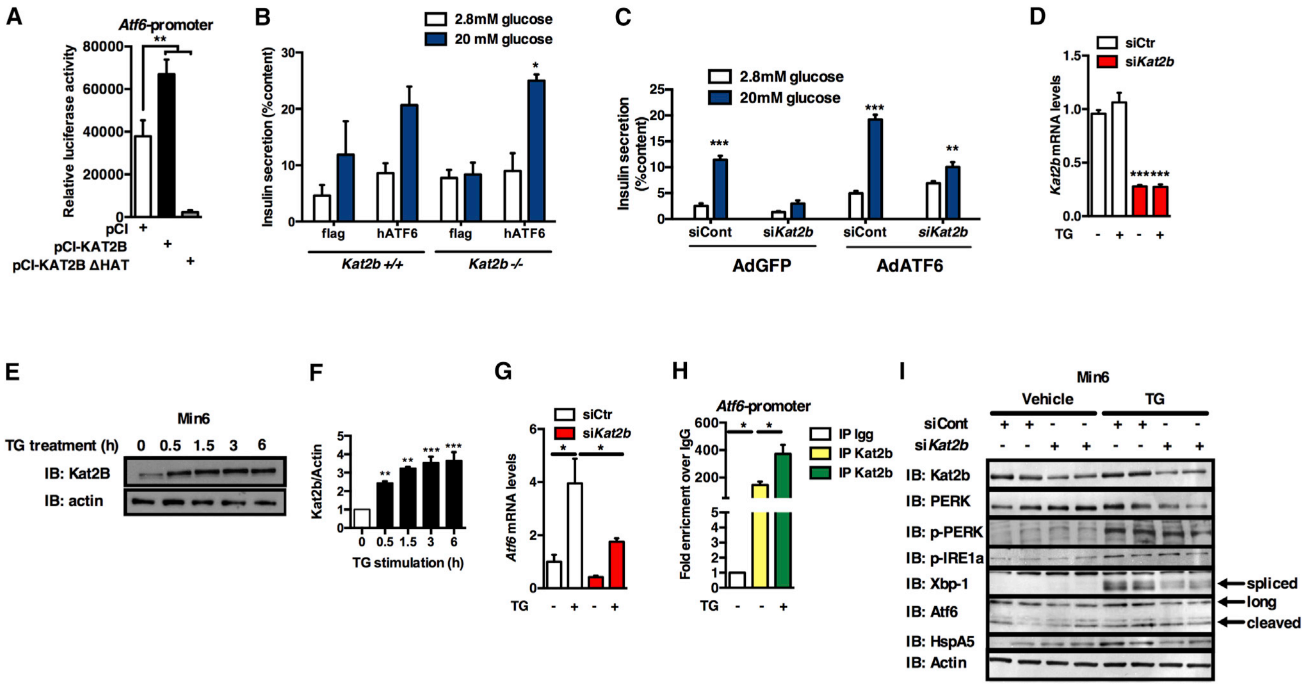

Figure 4. Kat2b Controls Several Branches of the UPR^{er} Signaling in Insulin-Producing Cells

(A) Min6 cells were transiently co-transfected with the Atf6 promoter luciferase construct in the absence (pCI) or presence of Kat2b (pCI-KAT2B) and catalically inactive KAT mutant (pCI-KAT2B ΔHAT). Results were normalized to β-galactosidase activity.

(B) Insulin secretion from *Kat2b* +/+ and −/− isolated islets transfected with pCDNA3-FLAG (flag) or pCDNA3-hATF6-FLAG (hATF6). Results were normalized to insulin content.

(C) Glucose-stimulated insulin secretion from control (*siCont*) and *Kat2b* silencing (*siKat2b*) in Min6 cells transduced with a control adenovirus (AdGFP) or encoding human ATF6 (AdATF6).

(D) mRNA levels of *Kat2b* in Min6 cells transfected with control (*siCont*) or *Kat2b* siRNA (*siKat2b*) and treated with vehicle (−) or thapsigargin (TG).

(E and F) Western blot assay (E) and quantification (F) showing increased Kat2b protein levels after treatment with 2.5 μM TG at different time points. Actin was used as a loading control. Quantification was performed using ImageJ software.

(G) mRNA levels of *Atf6* in Min6 cells transfected with control (*siCont*) or *Kat2b* siRNA (*siKat2b*) and treated with vehicle (−) or thapsigargin (TG).

(H) ChIP-qPCR demonstrating binding of Kat2b to the *Atf6* promoter in Min6 cells under basal and ER stress (TG) conditions.

(I) Western blot assay showing protein levels of several UPR^{er} markers in control (siCont) or *Kat2b* silenced (si*Kat2b*) Min6 cells treated or not with TG.

Data are shown as mean ± SEM. *p < 0.05, **p < 0.01, and ***p < 0.001.

decreased GSIS (Figures 5K and 5L) with a concomitant decrease in *ATF6* and *XBP1* mRNA levels (Figure 5M). Interestingly, analysis of ChIP-seq data from ENCODE (http://genome.ucsc.edu/ENCODE/) showed that KAT2B binds to numerous UPR^{er} genes in human cell lines, including *ATF6*, *XBP1*, *ATF4*, *HSPA5*, *DDIT3*, and *HERPUD2* (Figures S5–S7). These results are reminiscent of our ChIP-seq analysis in murine pancreatic islets. Formaldehyde-assisted isolation of regulatory elements (FAIRE)-sequencing (Giresi et al., 2007) and DNase-sequencing (Crawford et al., 2006) data further revealed that these UPR^{er} chromatin regions were associated with regulatory activities in pancreatic human islets (Figures S5–S7). In combination, these results strongly support the existence of a link between *KAT2B* and UPR^{er} gene expression in human islets and correlate defective *KAT2B* expression with T2D status in human pancreatic islets.

Our results suggest that KAT2B is likely to be an important mediator of insulin secretion and β cell adaptation during metabolic stress. Indeed, both germline and β cell-specific deletion of *Kat2b* in the mouse induces glucose intolerance and defective insulin secretion. Although we cannot rule out that Kat2b modulates other pathways involved in β cell function, our data from rodent models suggest that Kat2b directly regulates UPR^{er} gene expression. We found in human islets a robust association between the expression of this lysine acetyltransferase and crucial genes involved in insulin secretion and in β cell adaptive responses. By regulating UPR^{er} signaling pathways, KAT2B can be considered a critical transcriptional regulator of β cell function, especially after metabolic stress (Figure 6). The decrease of *KAT2B* expression in T2D islets and the inverse correlation with HbA1C levels further suggest a potential role for KAT2B during the onset of T2D.

During obesity, β cells need to adapt their insulin secretory capacity in response to nutrient overload by progressively expanding their islet cell mass (Weir and Bonner-Weir, 2004). Under diabetogenic conditions, *Kat2b* −/− mice are unable to compensate (Figure 1). *ob/ob* mice and hyperglycemic *db/db* mice display differential regulation of the adaptive UPR^{er} (Chan et al., 2013). The expression of UPR^{er} genes is induced in islets

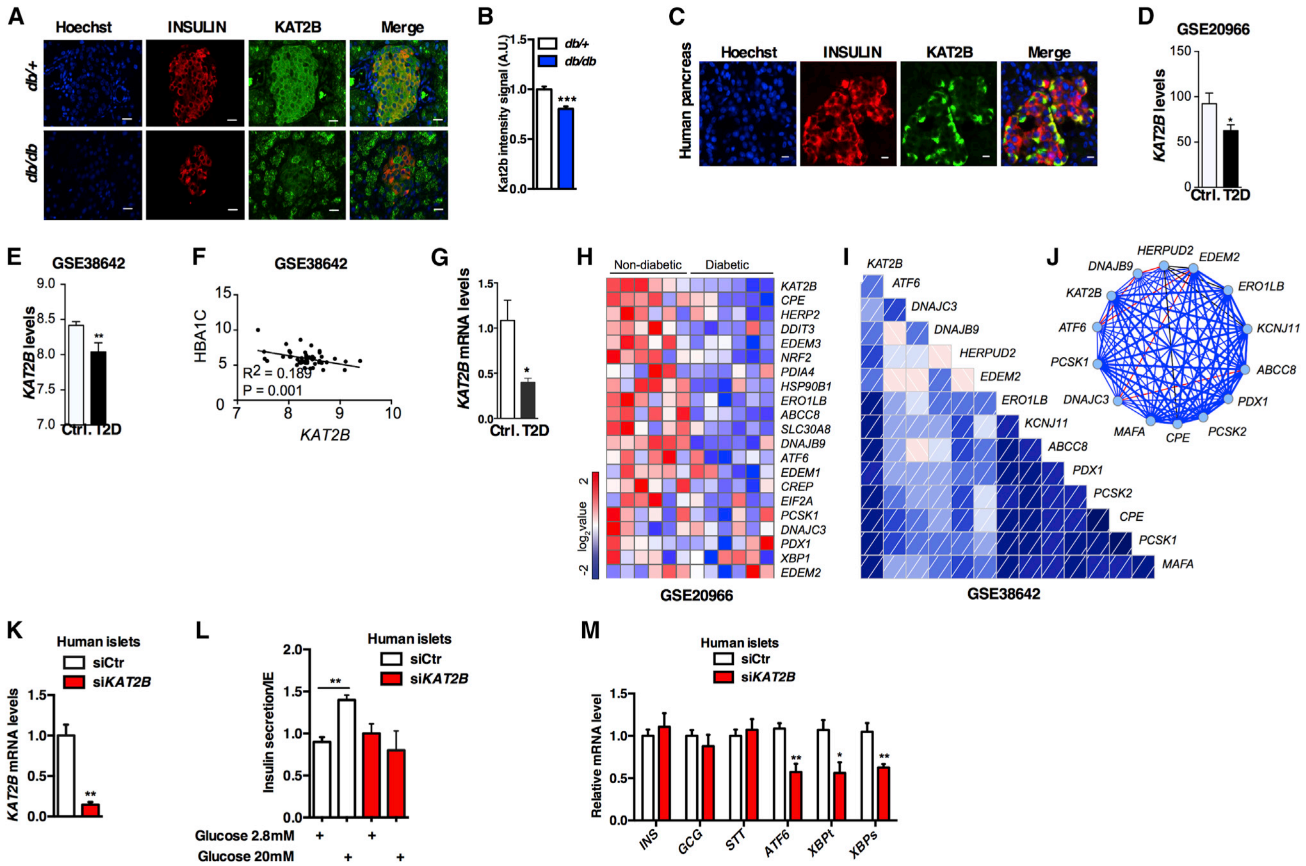

Figure 5. *Kat2B* Expression Is Decreased in *db/db* and Human T2D Islets

(A and B) Immunofluorescence microscopy analysis (A) and quantification (B) of pancreatic sections from 20 weeks old control (*db/+*) and obese diabetic *(db/db)* mice showing expression of Insulin and Kat2b. Analysis was performed on two independent experiments using 5 animals of each genotype and representative images are shown (scale bar, 20 μm).

(C) Immunostaining of pancreas sections demonstrating KAT2b expression in normal human β cells (insulin, red) and non-β cells (scale bar, 12.5μm).

(D and E) Correlation between *KAT2B* and T2D in humans. *KAT2B* expression is downregulated in pancreatic islets isolated from T2D patients. Analyses in (D) are based on human dataset GEO: GSE20966. The decreased expression of *KAT2B* in diabetic patients is confirmed in another independent human dataset in (E) (GEO: GSE38642).

(F) The expression levels of *KAT2B* are negatively correlated with Hba1C, a marker of T2D. Analyses are based on human dataset GEO: GSE38642.

(G) *KAT2B* mRNA levels in control and T2D human islets (n = 4).

(H) Custom gene-set analysis showing enrichment of ER stress and insulin production related transcripts downregulation in diabetic patients in human dataset GEO: GSE20966.

(I and J) To evaluate a possible link between *KAT2B* expression and key ER stress regulators and factors regulating insulin production, a correlation analysis with gene expression data from human pancreatic islets was performed using Pearson correlation coefficient. The positive correlation coefficient obtained allows us to establish a correlation matrix (I) and interaction network (J) showing correlations between *KAT2B* and genes involved in ER stress and insulin production. Positive and statistically significant Pearson's correlation coefficients are represented by blue edges, while negative coefficients are represented by red (r = 0.5–1.0).

(K) *KAT2B* mRNA levels from control (siCont) and *KAT2B* silenced (si*KAT2B*) human islets (n = 3).

(L) GSIS from control (siCont) and *KAT2B* silenced (si*KAT2B*) human islets (n = 3). Values were normalized per islet equivalent.

(M) mRNA levels of *INSULIN* (INS), *GLUCAGON* (GCG), *SOMATOSTATIN* (*STT*) and UPR^{er} genes in control (siCont) and *KAT2B* silenced (si*KAT2B*) human islets (n = 3).

Values in (B), (D), (E), (G), (K), (L), and (M) are expressed as means ± SEM; $^*p < 0.05$, $^{**}p < 0.01$, and $^{***}p < 0.001$.

of non-diabetic *ob/ob* mice, whereas it progressively decreases in diabetic *db/db* mice, linking UPR^{er} failure with progression to diabetes (Chan et al., 2013). Our observations that Kat2b levels are decreased in β cells of *db/db* mice suggest a molecular mechanism linking defective glucose homeostasis and UPR^{er} in these mice.

In conclusion, our study suggests that Kat2b contributes to the maintenance of efficient UPR^{er} levels in β cells to ensure an efficient adaptive response to stressful conditions, such as those inflicted by obesity and metabolic stress. Therefore, it is our expectation that the evidence presented here will guide the rationale and design of future therapeutic strategies by incorporating

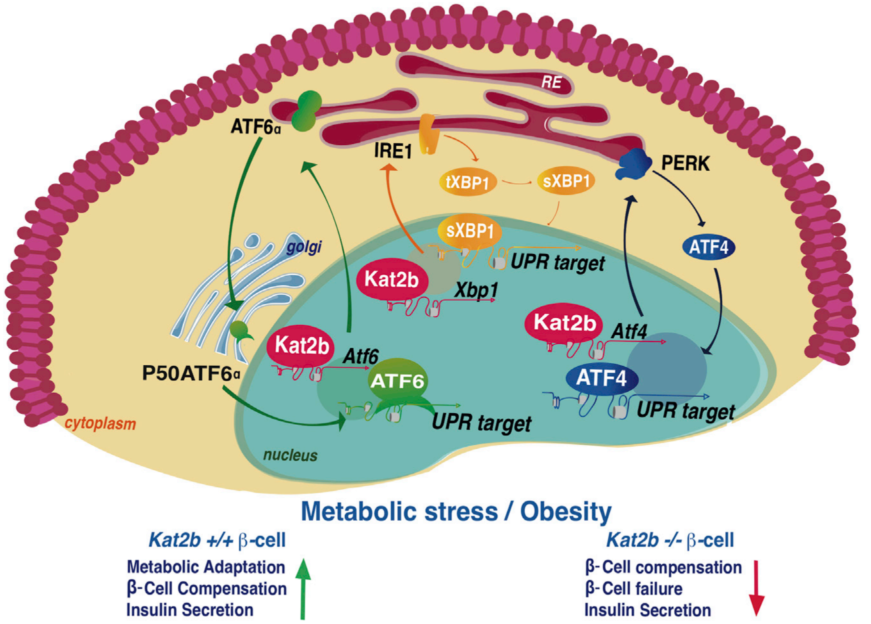

Figure 6. A Schematic Model Summarizing the Role of KAT2B in β Cells during Obesity and Metabolic Stress and Its Role in UPR^{er} Regulation

KAT2B-targeted drugs against T2D and related disorders such as obesity.

EXPERIMENTAL PROCEDURES

Materials and Oligonucleotides

Chemicals, unless stated otherwise, were purchased from Sigma-Aldrich. Anti-INS (ab7842), anti-ATF6 (ab11909), anti-KAT2B (ab96510 for immunofluorescence, ab12188 for ChIP), and Igg (ab37415 ChIP grade) antibodies were from Abcam; anti-KAT2B (sc-13124 for western blot), anti-actin (sc-1616), and anti-Xbp-1 antibodies were from Santa Cruz Biotechnology; anti-glucagon was from Sigma-Aldrich; and anti-PERK (C33E10), phospho-PERK (16F8), phospho-IRE1a (14C10), and anti-Hspa5 (C50B12) were from Cell Signaling. The oligonucleotides sequences used for various experiments are listed in Table S5. Plasmids with *Kat2b* cDNA were kindly provided by Drs. L.K. Linares and C. Gongora, and ATF6-pGL3 construct was kindly provided by Pr. Yoshida. The adenovirus encoding human ATF-6 has been described elsewhere (Sharma et al., 2015).

Animal Experiments

Mice were maintained according to European Union guidelines for the use of laboratory animals. In vivo experiments were performed in compliance with the French ethical guidelines for studies on experimental animals (animal house agreement no. A 59-35015, Authorization for Animal Experimentation no.59-350294, project approval by our local ethical comitttee no. CEEA 482012). Germline *Kat2b*-deficient mice were previously described (Duclot et al., 2010), and experiments were performed on CD1 strains. All experiments were performed with male mice. Mice were housed under a 12-hr light/dark cycle and given a regular chow (A04;Safe). For HFD studies, 5-week-old mice were placed on a D12492 diet (60% of calories from fat; Research Diet) for 13 weeks. Metabolic phenotyping experiments were performed according to the EMPRESS protocols. Intraperitoneal glucose and insulin tolerance tests (ITTs) were performed as previously described (Annicotte et al., 2009) on 16-hr-fasted animals for ipGTT and 5-hr-fasted animals for ITT. Glycemia was measured using the Accu-Check Performa (Roche Diagnostics). Circulating insulin levels were measured using the Ultrasensitive Insulin ELISA kit (Mercodia). Circulating Igf-1 levels were measured on fed animals using an Igf-1 ELISA kit (Sigma-Aldrich).

Kat2b floxed (*Kat2b*$^{L2/L2}$) mice were generated by homologous recombination in 129Sv embryonic stem (ES) cells according to standard procedures (Argmann et al., 2005). The karyotype was verified and several correctly targeted ES cell clones were injected into blastocysts from C57BL/6J mice. These blastocysts were transferred into pseudopregnant females, resulting in chimeric offspring that were mated to female C57BL/6J mice that express *Flp* recombinase under the control of the ubiquitous cytomegalovirus promoter (Rodríguez et al., 2000). Offspring that transmitted the mutated allele, in which the selection marker was excised, and that lost the *Flp* transgene (*Kat2b*$^{L2/WT}$ mice) were selected and backcrossed for over ten generations with C57BL/6J mice. The congenic mice carrying the floxed *Kat2b* allele were thereafter mated with rat insulin II promoter (RIP)-Cre mice (Herrera, 2000) and then further intercrossed to generate pure mutant *RIPcre*$^{Tg/0}$/*Kat2b*$^{L2/L2}$ mice. A PCR genotyping strategy was subsequently used to identify *RIPcre*$^{Tg/0}$/*Kat2b*+/+, *RIPcre*$^{Tg/0}$/*Kat2b*$^{L2/L2}$, and *RIPcre*$^{0/0}$/*Kat2b*$^{L2/L2}$ mice.

Immunofluorescence, Immunohistochemistry, and Morphometry

Immunofluorescence and immunohistochemistry were performed exactly as described previously (Annicotte et al., 2009; Blanchet et al., 2011). Pancreatic tissues were fixed in 10% formalin, embedded in paraffin, and sectioned at 5 μm. H&E staining was performed using classical protocols. For immunofluorescence microscopy analyses, after antigen retrieval using citrate buffer, 5-μm formalin-fixed pancreatic sections were incubated with the indicated antibodies. Immunofluorescence staining was revealed by using a fluorescein-isothiocyanate-conjugated anti-rabbit (for Kat2b; Life Technologies) or anti-guinea pig (for insulin co-staining with glucagon), Alexa-conjugated anti-mouse (for glucagon) or anti-guinea pig (for insulin co-staining with Kat2b) secondary antibodies. Nuclei were stained with Hoechst. For morphometric analysis, three to ten animals from each genotype were analyzed, and images were processed and quantified using ImageJ software by an observer blinded to experimental groups. Human pancreatic sections were obtained from Biochain.

Pancreatic Islet Studies

Human pancreatic tissue was harvested from brain-dead, non-diabetic, and T2D adult human donors (Table S4). Isolation and islet culture were performed as described elsewhere (Kerr-Conte et al., 2010). For mouse islet studies, pancreata were digested by type V collagenase (C9263; 1.5 mg/ml) for 20 min at 37°C as described previously (Annicotte et al., 2009). Briefly, after digestion and separation in a density gradient medium, islets were purified by handpicking under a macroscope. For insulin secretion tests, approximately ten islets were exposed to either 2.8 mM or 20 mM glucose in Krebs-Ringer bicarbonate HEPES buffer containing 0.5% fatty-acid-free BSA. Insulin released in the medium was measured 1 hr later using the Ultrasensitive Insulin ELISA kit. Data are expressed as a ratio of total insulin content. For mRNA and protein quantification, islets were isolated as described above and snap-frozen for further processing. For ATF-6 rescue experiments, isolated islets were transfected as described previously (Annicotte et al., 2009).

Cell Culture, Transfections, Adenoviral Transduction, and Treatments

Min6 cells were cultured in DMEM (Gibco) with 15% fetal bovine serum, 100 μg/ml penicillin-streptomycin, and 55 μM beta-mercaptoethanol. Cell were transfected with siRNA targeting mouse *Kat2b* ON-TARGETplus SMARTpool (Thermo Scientific) and mouse non-targeting negative controls using Dharmafect1 (GE Dharmacon). Mouse islets and Min6 cells were treated as described previously (Wali et al., 2014) with TUDCA (0.5 mM) and 4-PBA (2.5 mM) for 48 hr and subjected to GSIS. Min6 cells were treated with TG (0.5–2.5 μM; Sigma) to induce ER stress and then with BSA-conjugated palmitate (1.5 mM) for 24 hr. Transient transfection were performed using Lipofectamine 2000 (Life Technologies) following the manufacturer's instructions. Luciferase assays were performed 48 hr post-transfection and normalized to β-galactosidase activity. For rescue experiments using adenoviral infection, Min6 cells were transduced at a MOI of 50 for 4 hr; cells were then washed and cultured for 48 hr before GSIS tests. Experimental data as presented are means of at least three independent experimental experiments.

ChIP and ChIP Sequencing

ChIP-qPCR assays were performed as described previously (Annicotte et al., 2009). Briefly, proteins from Min6 cells were formaldehyde crosslinked to DNA. After homogeneization, lysis, and DNA sonication, proteins were immunoprecipitated using purified immunoglobulin G or anti-KAT2B antibodies. After washing, DNA-protein complexes were eluted and crosslinking was reversed by heating the samples at 65°C for 16 hr. DNA was then purified using a Macherey-Nagel NucleoSpin Gel and PCR purification kit, and ChIP-qPCR was performed using promoter-specific primers. All ChIPs and qPCRs were repeated three times.

ChIP assays were performed in triplicate on ~600 mouse isolated islets using the True MicroChIP kit (Diagenode) following the manufacturer's protocol. ChIP-seq libraries were prepared using NEBNext-Ultra kits (New England Biolabs) following the manufacturer's instructions. DNA libraries were quantified by Qubit (Invitrogen) and sequenced using a Hiseq 2500 instrument in single-end 50-bp reads (Illumina).

ChIP-Seq Data Analysis

ChIP-seq was performed in triplicate. Short DNA reads were aligned against the mouse mm9 reference genome using Bowtie 2 (Langmead and Salzberg, 2012). Only unique aligned reads were analyzed. The mapped replicates were merged and chromatin binding sites were identified using model-based analysis of ChIP-seq (MACS) (Zhang et al., 2008). Input DNA was used as a control, and parameters recommended for analysis of ChIP-seq data were applied (Feng et al., 2011). ChIP-seq experiments were visualized with the UCSC Genome browser as described elsewhere (Robertson et al., 2007). Peak summits were annotated to gene products by identifying the nearest RefSeq transcription start site using Peak2gene. Raw and processed ChIP-seq data have been deposited to Gene Expression Omnibus (GEO: GSE78860).

Public functional genomics data used in this study were downloaded from the GEO and are listed in Table S6. Human ChIP-seq data were obtained from ENCODE and visualized using the UCSC Genome browser as described above.

RNA Extraction, Measurements, and Profiling

Total RNA was extracted from cells and tissues using TRIzol reagent (Life Technologies) as described previously (Annicotte et al., 2009; Blanchet et al., 2012). mRNA expression was measured after reverse transcription by real-time qPCR with FastStart SYBR Green master mix (Roche) according to the manufacturer's recommendations and gene-specific oligonucleotides. Mouse real-time qPCR results were normalized to endogenous cyclophilin reference mRNA levels, and human results were normalized to TATA-box binding protein (*TBP*). Results are expressed as the relative mRNA level of a specific gene expression using the formula $2^{-\Delta Ct}$.

Protein Extracts and Immunoblot Analysis

Immunoblot was performed as described previously (Blanchet et al., 2012). Briefly, cells were washed using cold PBS and lysis was performed by using 50 mM Tris-HCl (pH 8), 137 mM NaCl, 10% glycerol, 1% NP-40 and phosphatase, protease, and deacetylase inhibitors (Sigma-Aldrich) on ice. Western blotting was performed using 30 μg of proteins loaded on SDS-PAGE precast gel (Bio-Rad). After electrotransfer, the membrane was blocked for 1 hr at room temperature with 5% nonfat milk in 0.1% Tween Tris-buffered saline (TTBS) buffer. Membranes were then incubated overnight at 4°C with primary antibodies as indicated in blocking buffer containing 5% nonfat milk at the dilution specified by the manufacturers. Membranes were then incubated with the secondary antibody conjugated with the enzyme horseradish peroxidase. The visualization of immunoreactive bands was performed using the enhanced chemiluminescence plus western blotting detection system (GE Healthcare). Quantification of protein signal intensity was performed by volume densitometry using ImageJ 1.47t software (NIH).

Human Islet Expression Data and Correlation Studies

To identify transcriptomic datasets from human pancreatic islets, GEO analysis from the NCBI was performed using "human islet T2D" as keywords and filtered with "Datasets." Three datasets were obtained, and two were selected based on the highest number of samples (GEO: GSE38642; Taneera et al., 2012; and GEO: GSE20966; Marselli et al., 2010). Datasets were downloaded from the GEO and analyzed with Gene Set Enrichment Analysis (GSEA; http://software.broadinstitute.org/gsea/) as described previously (Ryu et al., 2014). Correlation studies were based on Pearson's correlation coefficient and represented using R.

Statistical Analysis

Data are presented as mean ± SEM. Statistical analyses were performed using an unpaired two-tailed Student's t test, one-way ANOVA with a least significant difference Bonferroni post hoc test or two-way ANOVA with Bonferroni post hoc tests, as appropriate, using GraphPad Prism software. Differences were considered statistically significant at $p < 0.05$ (*$p < 0.05$, ** $p < 0.01$, and *** $p < 0.001$).

ACCESSION NUMBERS

The accession number for the raw and processed ChIP-seq data reported in this paper is GEO: GSE78860.

SUPPLEMENTAL INFORMATION

Supplemental Information includes seven figures and six tables can be found with this article online at http://dx.doi.org/10.1016/j.celrep.2016.03.079.

AUTHOR CONTRIBUTIONS

N.R. performed most of the experiments. P.D.D., X.G., E.S., S.A.H., E.D., A.B., C.C., and C.B. contributed to the in vivo and genomic experiments. N.R., H.Z., and O.S. performed bioinformatic analysis. L.Y. supervised statistical analyses. J.K.-C. performed human islet isolation from control and T2D donors. A.A., J.A., L.F., and P.F. contributed to study design, provided reagents and data, and discussed and interpreted the results from the study. J.A. and L.F. edited the manuscript. J.-S.A. designed the study, supervised the project, and contributed to experiments. N.R, A.A., P.F., and J.-S.A. wrote the manuscript.

ACKNOWLEDGMENTS

We thank Dr. Céline Gongora for providing us with the *Kat2b* −/− mice and Pr. Pedro Herrera for the Rip-Cre mice. We acknowledge Prs. Laurie H. Glimcher, Kenichi Yoshida, and Hiderou Yoshida for sharing UPR^{er} plasmids. We thank Dr. Laura C. Alonso for providing us with the hATF-6 adenovirus. We thank members of UMR 8199 for technical assistance, in particular Carine de Bettignies, Laure Rolland, Audrey Leloire, and Emmanuel Vaillant. We acknowledge Pr. François Pattou for critical reading of the manuscript. We thank Estelle Leborgne for help with illustrations. The authors thank the High Technology animal facility of IMPRT-IFR 114, especially Yann Lepage, Ludovic Mercier, Kelly Timmerman, Mélanie Besegher, and Delphine Taillieu, for animal care. We acknowledge Dr. Emilie Caron for helpful discussions. We thank the Department of Histology from the Lille Medicine Faculty, in particular M.H. Gevaert and R.M. Siminski, for histological preparations. We are indebted to the Réseau d'Histologie Expérimentale de Montpellier (RHEM) network (IFR122, France) for histology and, in particular, for tissue and slide preparations. This work was supported by grants from the European Genomic Institute for Diabetes (EGID; ANR-10-LABX-46 to A.A., P.F., and J.-S.A.), the European Commission, the European Research Council (GEPIDIAB 294785 to P.F.), INSERM, the CNRS, Association pour la Recherche sur le Diabète (to J.-S.A.), Lille2 University (to N.R., X.G., E.S. and J-S.A.), Conseil Régional Nord-Pas de Calais and Métropole Européenne de Lille (to N.R., X.G., and J.-S.A.), FEDER (Fonds Européen de Développement Régional; to N.R., P.F., and J.-S.A.), Société Francophone du Diabète/Servier (to S.A.H. and J.-S.A), the Ecole Polytechnique Fédérale de Lausanne (to J.A.), the National Institutes of Health (R01AG043930 to J.A.), Krebsforschung Schweiz (KFS-3082-02-2013 to J.A.), Systems X (SySX.ch 2013/153 to J.A.), and SNSF (31003A-140780 to J.A.). H.Z. is supported by a fellowship from Carigest, and J.A. is the Nestlé Chair in Energy Metabolism.

Received: September 2, 2015
Revised: February 2, 2016
Accepted: March 22, 2016
Published: April 21, 2016

REFERENCES

Annicotte, J.S., Blanchet, E., Chavey, C., Iankova, I., Costes, S., Assou, S., Teyssier, J., Dalle, S., Sardet, C., and Fajas, L. (2009). The CDK4-pRB-E2F1 pathway controls insulin secretion. Nat. Cell Biol. *11*, 1017–1023.

Argmann, C.A., Chambon, P., and Auwerx, J. (2005). Mouse phenogenomics: the fast track to "systems metabolism". Cell Metab. *2*, 349–360.

Back, S.H., and Kaufman, R.J. (2012). Endoplasmic reticulum stress and type 2 diabetes. Annu. Rev. Biochem. *81*, 767–793.

Blanchet, E., Annicotte, J.-S., Lagarrigue, S., Aguilar, V., Clapé, C., Chavey, C., Fritz, V., Casas, F., Apparailly, F., Auwerx, J., and Fajas, L. (2011). E2F transcription factor-1 regulates oxidative metabolism. Nat. Cell Biol. *13*, 1146–1152.

Blanchet, E., Annicotte, J.S., Pradelli, L.A., Hugon, G., Matecki, S., Mornet, D., Rivier, F., and Fajas, L. (2012). E2F transcription factor-1 deficiency reduces pathophysiology in the mouse model of Duchenne muscular dystrophy through increased muscle oxidative metabolism. Hum. Mol. Genet. *21*, 3910–3917.

Chan, J.Y., Luzuriaga, J., Bensellam, M., Biden, T.J., and Laybutt, D.R. (2013). Failure of the adaptive unfolded protein response in islets of obese mice is linked with abnormalities in β-cell gene expression and progression to diabetes. Diabetes *62*, 1557–1568.

Cnop, M., Foufelle, F., and Velloso, L.A. (2012). Endoplasmic reticulum stress, obesity and diabetes. Trends Mol. Med. *18*, 59–68.

Crawford, G.E., Holt, I.E., Whittle, J., Webb, B.D., Tai, D., Davis, S., Margulies, E.H., Chen, Y., Bernat, J.A., Ginsburg, D., et al. (2006). Genome-wide mapping of DNase hypersensitive sites using massively parallel signature sequencing (MPSS). Genome Res. *16*, 123–131.

Duclot, F., Meffre, J., Jacquet, C., Gongora, C., and Maurice, T. (2010). Mice knock out for the histone acetyltransferase p300/CREB binding protein-associated factor develop a resistance to amyloid toxicity. Neuroscience *167*, 850–863.

Eizirik, D.L., and Cnop, M. (2010). ER stress in pancreatic beta cells: the thin red line between adaptation and failure. Sci. Signal. *3*, pe7.

Engin, F., Nguyen, T., Yermalovich, A., and Hotamisligil, G.S. (2014). Aberrant islet unfolded protein response in type 2 diabetes. Sci. Rep. *4*, 4054.

Feng, J., Liu, T., and Zhang, Y. (2011). Using MACS to identify peaks from ChIP-seq data. Curr. Protoc. Bioinformatics *Chapter 2*, Unit 2.14.

Fonseca, S.G., Gromada, J., and Urano, F. (2011). Endoplasmic reticulum stress and pancreatic β-cell death. Trends Endocrinol. Metab. *22*, 266–274.

Giresi, P.G., Kim, J., McDaniell, R.M., Iyer, V.R., and Lieb, J.D. (2007). FAIRE (Formaldehyde-Assisted Isolation of Regulatory Elements) isolates active regulatory elements from human chromatin. Genome Res. *17*, 877–885.

Haumaitre, C., Lenoir, O., and Scharfmann, R. (2008). Histone deacetylase inhibitors modify pancreatic cell fate determination and amplify endocrine progenitors. Mol. Cell. Biol. *28*, 6373–6383.

Herrera, P.L. (2000). Adult insulin- and glucagon-producing cells differentiate from two independent cell lineages. Development *127*, 2317–2322.

Hetz, C. (2012). The unfolded protein response: controlling cell fate decisions under ER stress and beyond. Nat. Rev. Mol. Cell Biol. *13*, 89–102.

Kelly, D.P., and Scarpulla, R.C. (2004). Transcriptional regulatory circuits controlling mitochondrial biogenesis and function. Genes Dev. *18*, 357–368.

Kennedy, J., Katsuta, H., Jung, M.H., Marselli, L., Goldfine, A.B., Balis, U.J., Sgroi, D., Bonner-Weir, S., and Weir, G.C. (2010). Protective unfolded protein response in human pancreatic beta cells transplanted into mice. PLoS ONE *5*, e11211.

Kerr-Conte, J., Vandewalle, B., Moerman, E., Lukowiak, B., Gmyr, V., Arnalsteen, L., Caiazzo, R., Sterkers, A., Hubert, T., Vantyghem, M.C., and Pattou, F. (2010). Upgrading pretransplant human islet culture technology requires human serum combined with media renewal. Transplantation *89*, 1154–1160.

Langmead, B., and Salzberg, S.L. (2012). Fast gapped-read alignment with Bowtie 2. Nat. Methods *9*, 357–359.

Laybutt, D.R., Preston, A.M., Akerfeldt, M.C., Kench, J.G., Busch, A.K., Biankin, A.V., and Biden, T.J. (2007). Endoplasmic reticulum stress contributes to beta cell apoptosis in type 2 diabetes. Diabetologia *50*, 752–763.

Lenoir, O., Flosseau, K., Ma, F.X., Blondeau, B., Mai, A., Bassel-Duby, R., Ravassard, P., Olson, E.N., Haumaitre, C., and Scharfmann, R. (2011). Specific control of pancreatic endocrine β- and δ-cell mass by class IIa histone deacetylases HDAC4, HDAC5, and HDAC9. Diabetes *60*, 2861–2871.

Lundh, M., Christensen, D.P., Damgaard Nielsen, M., Richardson, S.J., Dahllöf, M.S., Skovgaard, T., Berthelsen, J., Dinarello, C.A., Stevenazzi, A., Mascagni, P., et al. (2012). Histone deacetylases 1 and 3 but not 2 mediate cytokine-induced beta cell apoptosis in INS-1 cells and dispersed primary islets from rats and are differentially regulated in the islets of type 1 diabetic children. Diabetologia *55*, 2421–2431.

Marselli, L., Thorne, J., Dahiya, S., Sgroi, D.C., Sharma, A., Bonner-Weir, S., Marchetti, P., and Weir, G.C. (2010). Gene expression profiles of Beta-cell enriched tissue obtained by laser capture microdissection from subjects with type 2 diabetes. PLoS ONE *5*, e11499.

Maurice, T., Duclot, F., Meunier, J., Naert, G., Givalois, L., Meffre, J., Célérier, A., Jacquet, C., Copois, V., Mechti, N., et al. (2008). Altered memory capacities and response to stress in p300/CBP-associated factor (PCAF) histone acetylase knockout mice. Neuropsychopharmacology *33*, 1584–1602.

Menzies, K.J., Zhang, H., Katsyuba, E., and Auwerx, J. (2016). Protein acetylation in metabolism - metabolites and cofactors. Nat. Rev. Endocrinol. *12*, 43–60.

Mihaylova, M.M., and Shaw, R.J. (2013). Metabolic reprogramming by class I and II histone deacetylases. Trends Endocrinol. Metab. *24*, 48–57.

Mouchiroud, L., Eichner, L.J., Shaw, R.J., and Auwerx, J. (2014). Transcriptional coregulators: fine-tuning metabolism. Cell Metab. *20*, 26–40.

Muoio, D.M., and Newgard, C.B. (2008). Mechanisms of disease:Molecular and metabolic mechanisms of insulin resistance and beta-cell failure in type 2 diabetes. Nat. Rev. Mol. Cell Biol. *9*, 193–205.

Plaisance, V., Rolland, L., Gmyr, V., Annicotte, J.S., Kerr-Conte, J., Pattou, F., and Abderrahmani, A. (2014). The class I histone deacetylase inhibitor MS-275 prevents pancreatic beta cell death induced by palmitate. J. Diabetes Res. *2014*, 195739.

Rabhi, N., Salas, E., Froguel, P., and Annicotte, J.S. (2014). Role of the unfolded protein response in β cell compensation and failure during diabetes. J. Diabetes Res. *2014*, 795171.

Robertson, G., Hirst, M., Bainbridge, M., Bilenky, M., Zhao, Y., Zeng, T., Euskirchen, G., Bernier, B., Varhol, R., Delaney, A., et al. (2007). Genome-wide profiles of STAT1 DNA association using chromatin immunoprecipitation and massively parallel sequencing. Nat. Methods *4*, 651–657.

Rodríguez, C.I., Buchholz, F., Galloway, J., Sequerra, R., Kasper, J., Ayala, R., Stewart, A.F., and Dymecki, S.M. (2000). High-efficiency deleter mice show that FLPe is an alternative to Cre-loxP. Nat. Genet. *25*, 139–140.

Ryu, D., Jo, Y.S., Lo Sasso, G., Stein, S., Zhang, H., Perino, A., Lee, J.U., Zeviani, M., Romand, R., Hottiger, M.O., et al. (2014). A SIRT7-dependent acetylation switch of GABPβ1 controls mitochondrial function. Cell Metab. *20*, 856–869.

Sampley, M.L., and Ozcan, S. (2012). Regulation of insulin gene transcription by multiple histone acetyltransferases. DNA Cell Biol. *31*, 8–14.

Sharma, R.B., O'Donnell, A.C., Stamateris, R.E., Ha, B., McCloskey, K.M., Reynolds, P.R., Arvan, P., and Alonso, L.C. (2015). Insulin demand regulates β cell number via the unfolded protein response. J. Clin. Invest. *125*, 3831–3846.

Taneera, J., Lang, S., Sharma, A., Fadista, J., Zhou, Y., Ahlqvist, E., Jonsson, A., Lyssenko, V., Vikman, P., Hansson, O., et al. (2012). A systems genetics approach identifies genes and pathways for type 2 diabetes in human islets. Cell Metab. *16*, 122–134.

Tang, C., Koulajian, K., Schuiki, I., Zhang, L., Desai, T., Ivovic, A., Wang, P., Robson-Doucette, C., Wheeler, M.B., Minassian, B., et al. (2012). Glucose-induced beta cell dysfunction in vivo in rats: link between oxidative stress and endoplasmic reticulum stress. Diabetologia *55*, 1366–1379.

Usui, M., Yamaguchi, S., Tanji, Y., Tominaga, R., Ishigaki, Y., Fukumoto, M., Katagiri, H., Mori, K., Oka, Y., and Ishihara, H. (2012). Atf6α-null mice are glucose intolerant due to pancreatic β-cell failure on a high-fat diet but partially resistant to diet-induced insulin resistance. Metabolism *61*, 1118–1128.

Wali, J.A., Rondas, D., McKenzie, M.D., Zhao, Y., Elkerbout, L., Fynch, S., Gurzov, E.N., Akira, S., Mathieu, C., Kay, T.W., et al. (2014). The proapoptotic BH3-only proteins Bim and Puma are downstream of endoplasmic reticulum and mitochondrial oxidative stress in pancreatic islets in response to glucotoxicity. Cell Death Dis. *5*, e1124.

Walter, P., and Ron, D. (2011). The unfolded protein response: from stress pathway to homeostatic regulation. Science *334*, 1081–1086.

Wang, S., and Kaufman, R.J. (2012). The impact of the unfolded protein response on human disease. J. Cell Biol. *197*, 857–867.

Weir, G.C., and Bonner-Weir, S. (2004). Five stages of evolving beta-cell dysfunction during progression to diabetes. Diabetes *53* (*Suppl 3*), S16–S21.

Yamauchi, T., Yamauchi, J., Kuwata, T., Tamura, T., Yamashita, T., Bae, N., Westphal, H., Ozato, K., and Nakatani, Y. (2000). Distinct but overlapping roles of histone acetylase PCAF and of the closely related PCAF-B/GCN5 in mouse embryogenesis. Proc. Natl. Acad. Sci. USA *97*, 11303–11306.

Zhang, Y., Liu, T., Meyer, C.A., Eeckhoute, J., Johnson, D.S., Bernstein, B.E., Nusbaum, C., Myers, R.M., Brown, M., Li, W., and Liu, X.S. (2008). Model-based analysis of ChIP-Seq (MACS). Genome Biol. *9*, R137.

Zhao, S., Xu, W., Jiang, W., Yu, W., Lin, Y., Zhang, T., Yao, J., Zhou, L., Zeng, Y., Li, H., et al. (2010). Regulation of cellular metabolism by protein lysine acetylation. Science *327*, 1000–1004.

Cell Reports, Volume *15*

Supplemental Information

KAT2B Is Required for Pancreatic Beta Cell Adaptation to Metabolic Stress by Controlling the Unfolded Protein Response

Nabil Rabhi, Pierre-Damien Denechaud, Xavier Gromada, Sarah Anissa Hannou, Hongbo Zhang, Talha Rashid, Elisabet Salas, Emmanuelle Durand, Olivier Sand, Amélie Bonnefond, Loic Yengo, Carine Chavey, Caroline Bonner, Julie Kerr-Conte, Amar Abderrahmani, Johan Auwerx, Lluis Fajas, Philippe Froguel, and Jean-Sébastien Annicotte

Supplemental informations

Supplemental figures and legends

Supplemental Figure S1, related to Figure 1. Effect of *Kat2b* deficiency on β−cell mass and function. (A-B) Body weight **(A)** and size **(B) of** *Kat2b +/+ and -/-* mice under chow. **(C-D**) Liver mRNA **(C)** and circulating Igf-1 **(D)** levels in *Kat2b +/+ and -/-* mice. **(E)** Body weight gain under high fat diet feeding of *Kat2b +/+ and -/-* mice. **(F-G)** Immunofluorescent experiments on pancreatic sections from *Kat2b +/+ and -/-* mice. IgGs **(F)** and *Kat2b -/-* **(G)** sections were used as negative controls for Kat2B antibody validation (scale bar, 12.5µm). **(H)** Insulin content of *Kat2b +/+ and -/-* isolated islets. **(I)** mRNA levels of *Kat2b* expression after silencing of *Kat2b* by siRNA in Min6 cells. **(J)** Glucose stimulated insulin secretion assay on *Kat2b* silenced Min6 cells. **(K)** Representative haematoxylin and eosin stainings on pancreatic sections of mice fed normal chow or HFD (scale bar, 200µm). **(L)** Islet areas were normalized to total pancreatic areas and were distributed following their frequency from mice fed chow or HFD as indicated. **(M)** Immunostaining of pancreas sections showing nuclei labeling (Hoechst), insulin positive β cells and glucagon positive α cells on *Kat2b* +/+ and -/- mice fed chow and HFD (scale bar, 100µm). **(N-O)** Quantification of glucagon **(N)** and insulin **(O)** positive cells per islet. **(P)** Circulating glucagon levels in *Kat2b* +/+ and -/- mice fed chow. Data are shown as mean ± SEM. ** *p* <0.01 and *** *p* <0.001.

Supplemental Figure S2, related to Figure 2. β−cell specific invalidation of *Kat2b* in mice. (A) Gene targeting and conditional deletion of exon 11 of the *Kat2b* gene. Maps of the *Kat2b* genomic locus (*Kat2b +/+)*, the floxed allele with (+neo, target allele) or without the neomycin cassette (−neo, *Kat2b* $^{ß+/+}$), and after Cre recombination (*Kat2b* $^{ß-/-}$) are represented. **(B)** Relative expression of *Kat2b* gene in different tissues obtained from *Kat2b* $^{ß+/+}$ and *Kat2b* $^{ß-/-}$ mice. All values represent mean ± SEM. * *p* <0.05.

Supplemental Figure S3, related to Figure 3. *Kat2b* modulates UPR^{er} signaling in murine pancreatic islets. (A) Relative expression of relevant β-cell enriched genes in islets isolated from *Kat2b +/+ and -/-* mice fed a chow diet. **(B)** ChIP-seq analysis in mouse islets identifies chromatin binding of Kat2b to its target genes *Xbp1*, *Hspa5* (*BiP), Atf4* and *Atf6* involved in the UPR^{er}, as described in the Experimental Procedures section. Briefly, after sequencing, reads were aligned to a reference genome, peaks were visualized using UCSC Genome browser to identify Kat2b bound genes. **(C)** Effects of TUDCA and 4-PBA treatments on glucose-stimulated insulin secretion from control (*siCont*) and *Kat2b* silencing (*siKat2b*) in Min6 cells. **(D)** Relative expression of relevant β-cell enriched genes in islets isolated from *Kat2b +/+ and -/-* mice fed HFD. **(E-F)** Relative expression of relevant UPR^{er} **(E)** and β-cell function **(F)** genes in control (siCont) or *Kat2b* silenced (si*Kat2b*) Min6 cells. All values represent mean ± SEM. * p <0.05; ** p <0.01 and *** p <0.001.

Supplementary Figure S4, related to Figure 4. Validation of ATF6 rescue experiments in Min6 cells and increased Kat2b protein levels upon stress. (A) Relative expression of the human *ATF6* gene in islets isolated from *Kat2b +/+ and -/-* mice transiently transfected with an empty vector (pCI) or an expression vector expressing human *ATF6* (pCI-ATF6). **(B)** Western blot assay showing the protein levels of Kat2b, ATF6 and actin from control (*siCont*) and *Kat2b* silencing (*siKat2b*) in Min6 cells transduced with an control adenovirus (AdGFP) or encoding human ATF6 (AdATF6). **(C-D)** Western blot assay showing increased Kat2b protein levels after TG at different concentrations **(C)** or 1.5mM palmitate treatment for 24 hours **(D)**. Actin was used as a loading control. **(E-F)** ChIP-qPCR demonstrating global acetylation of histone H3 (AcH3), acetylation on lysine 9 (AcH3K9) or lysine 14 (AcH3K14) of the *Atf6* **(E)** and *Pdx1* **(F)** promoters in control (siCont) or *Kat2b* silenced (si*Kat2b*) Min6 cells.

Supplementary Figure S5 to S7, related to Figure 5. KAT2B binds to chromatin of UPR^{er} genes in human cell lines. (A-B) ChIP-seq analysis from ENCODE data showing KAT2B binding and open chromatin regions associated with regulatory activity (DNase1 (Crawford et al., 2006) and FAIRE-seq (Giresi et al., 2007)) on human **(S5A)** *ATF6*, **(S5B)** *XBP1,* **(S6A)** *ATF4,* **(S6B)** *HSPA5,* **(S7A)** *DDIT3* and **(S7D)** HERPUD2 genes. KAT2B chip-seq peaks were obtained from GSM393947 (T lymphocytes) and GSM831007 (K562 cell line). DNAse1-seq (GSM586891) and FAIRE-seq (GSM1026917) ChIP-seq data were obtained from human pancreatic islets. Red arrows indicate the direction of transcription. Encode data were visualized using the UCSC Genome browser to identify peak profiles and their corresponding genes.

Supplemental tables

Supplemental Table S1, related to Figure 3. DNA-responsive element bound by Kat2b in isolated islets.

Supplemental Table S2, related to Figure 3. Gene ontology analysis of ChIP-seq data.

Supplemental Table S3, related to Figure 3. List of Kat2b target genes involved in UPR^{er} obtained after functional enrichment analysis of ChIP-seq data using g:profiler.

Supplemental Table S4, related to Figure 5. Donor informations

Supplemental Table S5, related to Figure 2, 3, 4, 5, S1, S2, S3 and S4. List of oligonucleotides used in qRT-PCR and ChIP-qPCR analyses.

Supplemental Table S6, related to Figure 5, S5, S6 and S7. List of data sets used in bioinformatical analyses.

Rabhi *et al.*, supplemental Figure 1

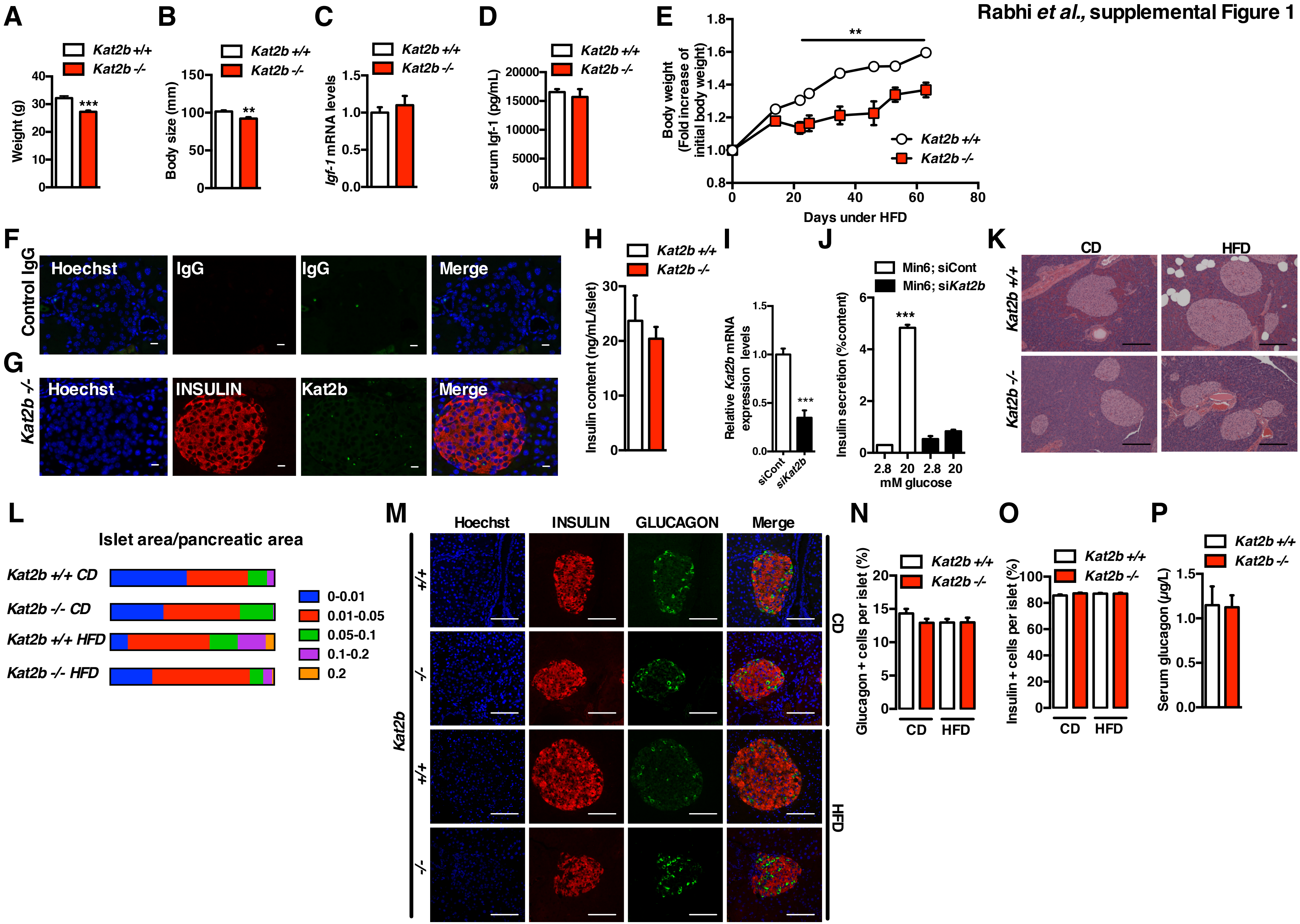

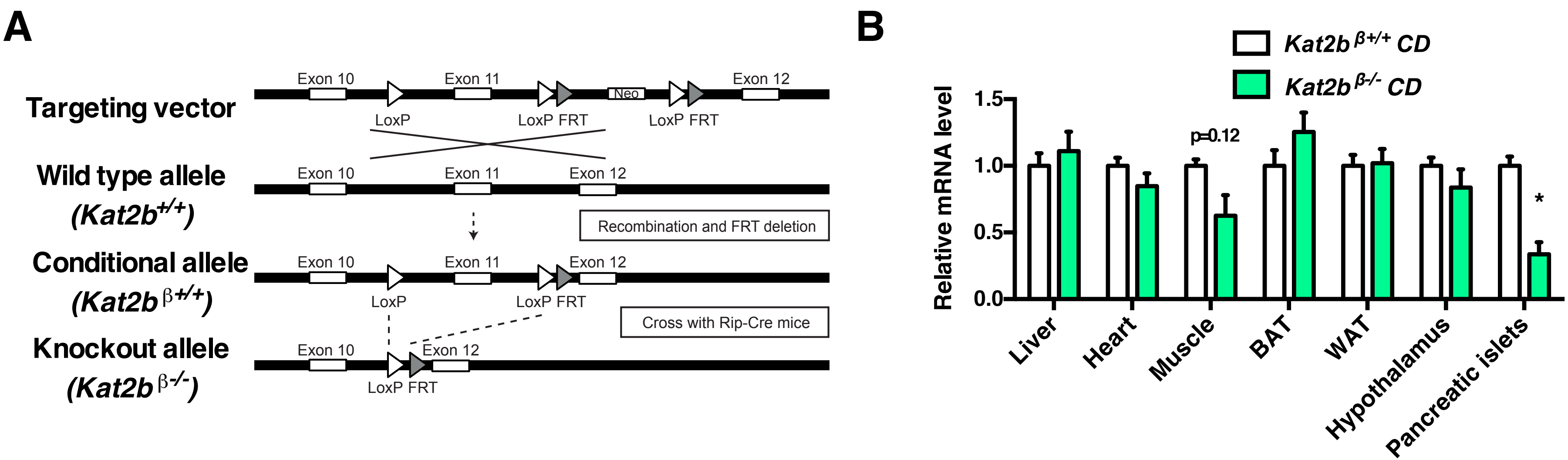
A
Targeting vector
Exon 10
Exon 11
Exon 12
LoxP
LoxP FRT
Neo
LoxP FRT
Wild type allele
(Kat2b+/+)
Exon 10
Exon 11
Exon 12
Recombination and FRT deletion
Conditional allele
(Kat2b β+/+)
Exon 10
Exon 11
Exon 12
LoxP
LoxP FRT
Cross with Rip-Cre mice
Knockout allele
(Kat2b β-/-)
Exon 10
Exon 12
LoxP FRT
B
Kat2b β+/+ CD
Kat2b β-/- CD
Relative mRNA level
1.5
1.0
0.5
0.0
p=0.12
*
Liver
Heart
Muscle
BAT
WAT
Hypothalamus
Pancreatic islets

Rabhi *et al.*, supplemental Figure 3

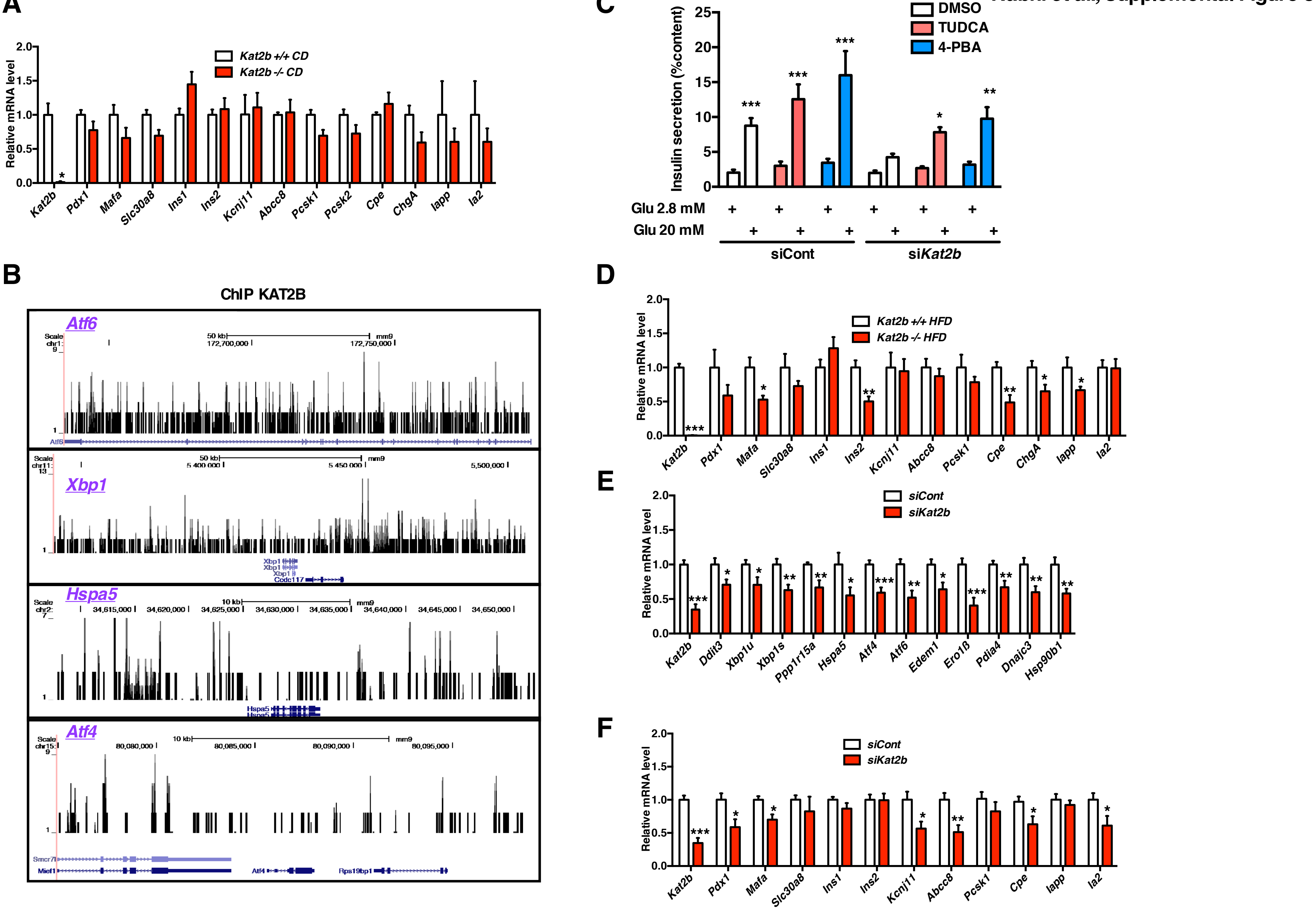

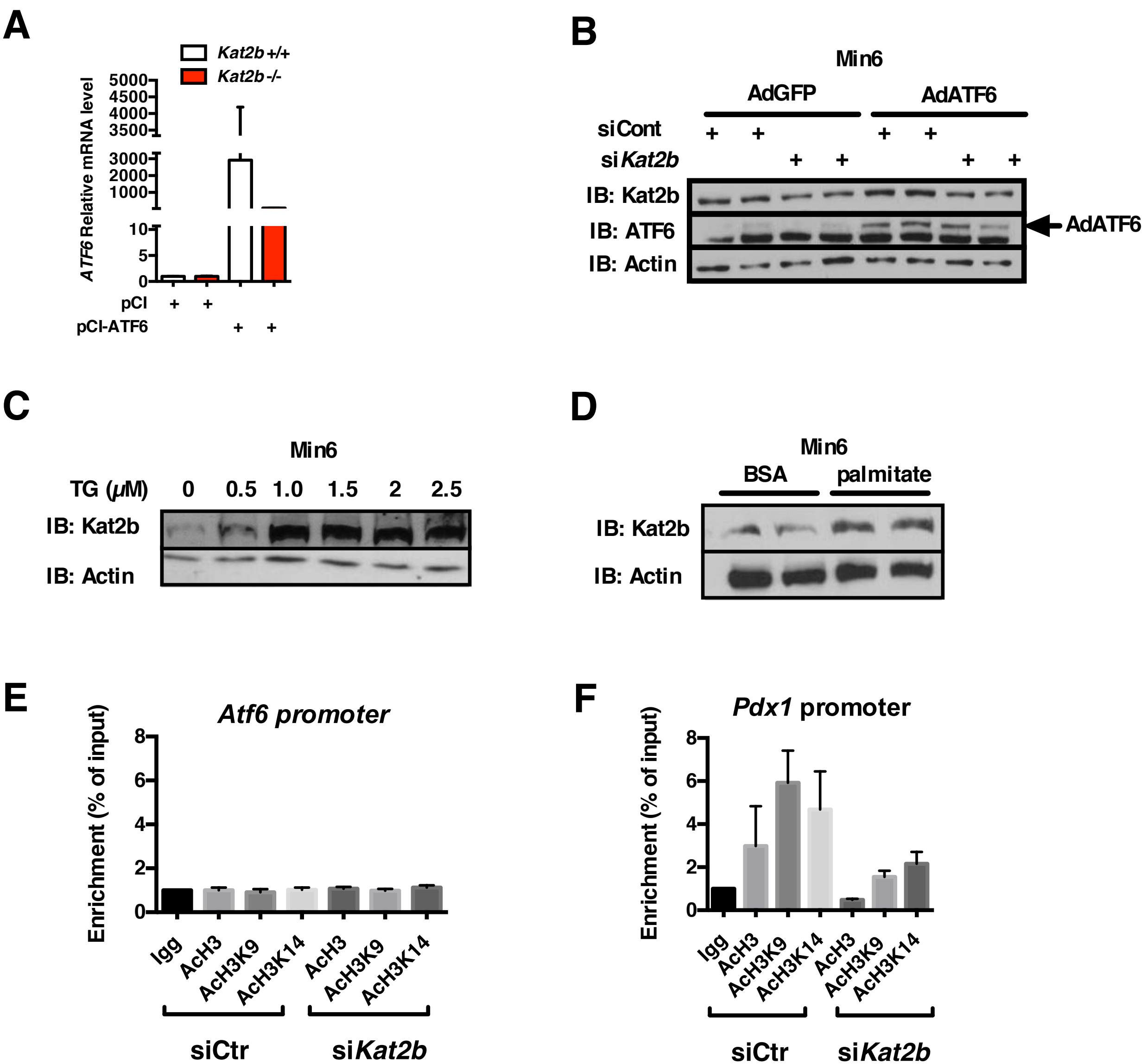
A
Kat2b +/+
Kat2b -/-
ATF6 Relative mRNA level
5000
4500
4000
3500
3000
2000
1000
10
5
0
pCI
pCI-ATF6
B
Min6
AdGFP
AdATF6
siCont
siKat2b
IB: Kat2b
IB: ATF6
IB: Actin
AdATF6
C
Min6
TG (μM) 0 0.5 1.0 1.5 2 2.5
IB: Kat2b
IB: Actin
D
Min6
BSA
palmitate
IB: Kat2b
IB: Actin
E
Atf6 promoter
Enrichment (% of input)
8
6
4
2
0
Igg
AcH3
AcH3K9
AcH3K14
AcH3
AcH3K9
AcH3K14
siCtr
siKat2b
F
Pdx1 promoter
Enrichment (% of input)
8
6
4
2
0
Igg
AcH3
AcH3K9
AcH3K14
AcH3
AcH3K9
AcH3K14
siCtr
siKat2b

Rabhi *et al.*, supplemental Figure 5

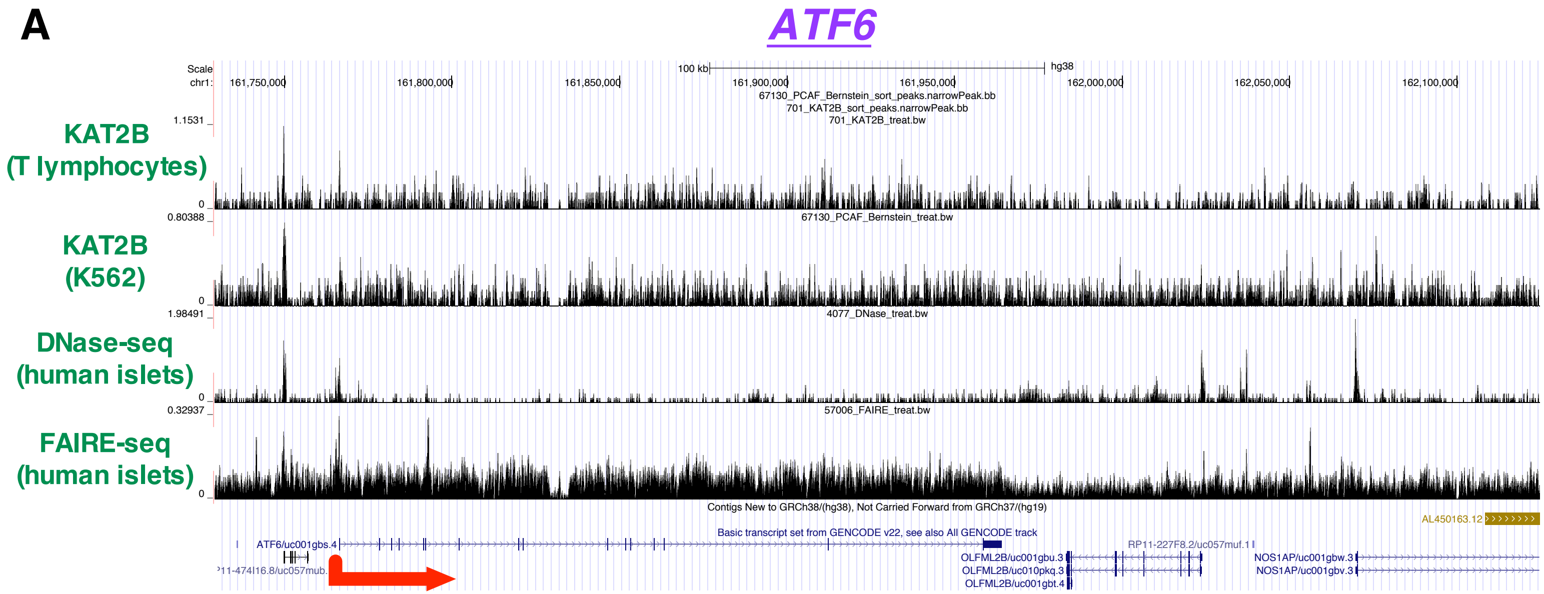

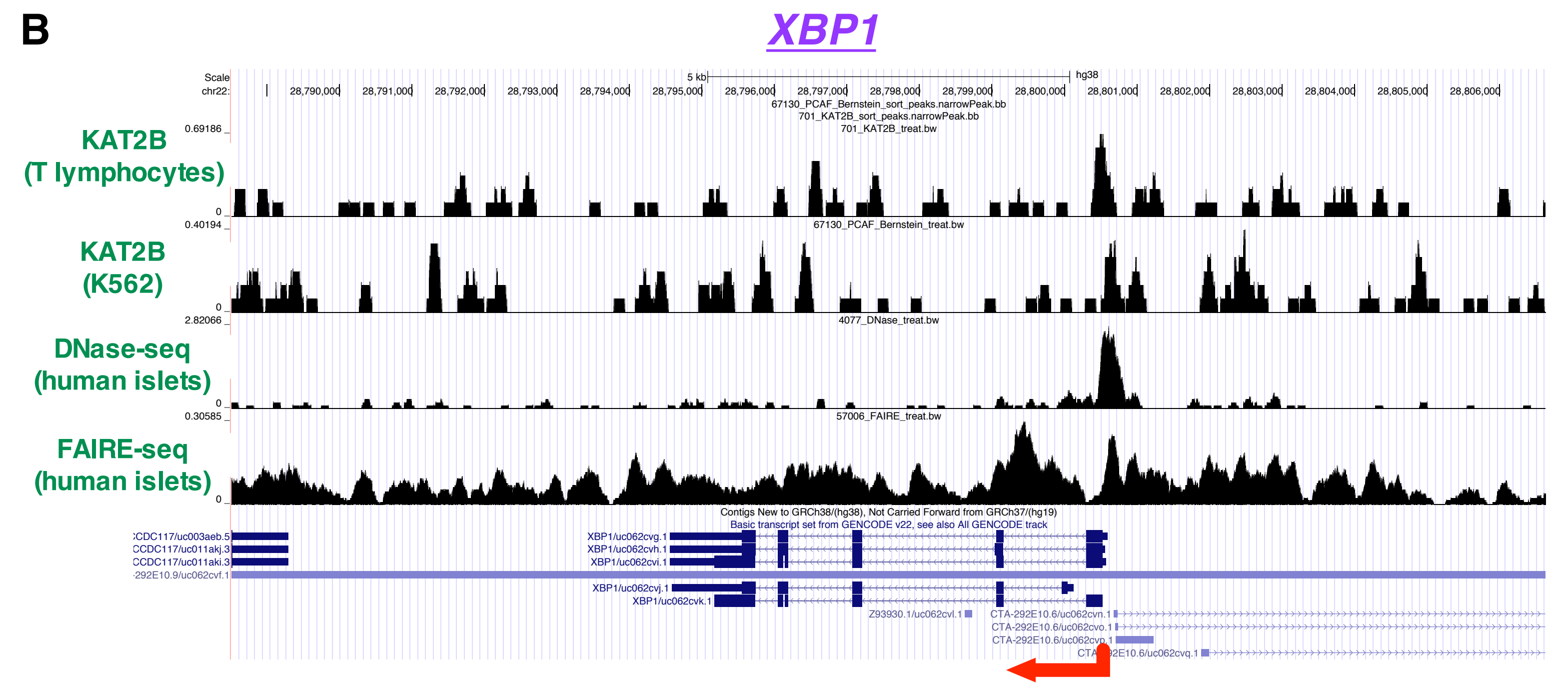

Rabhi *et al.*, supplemental Figure 6

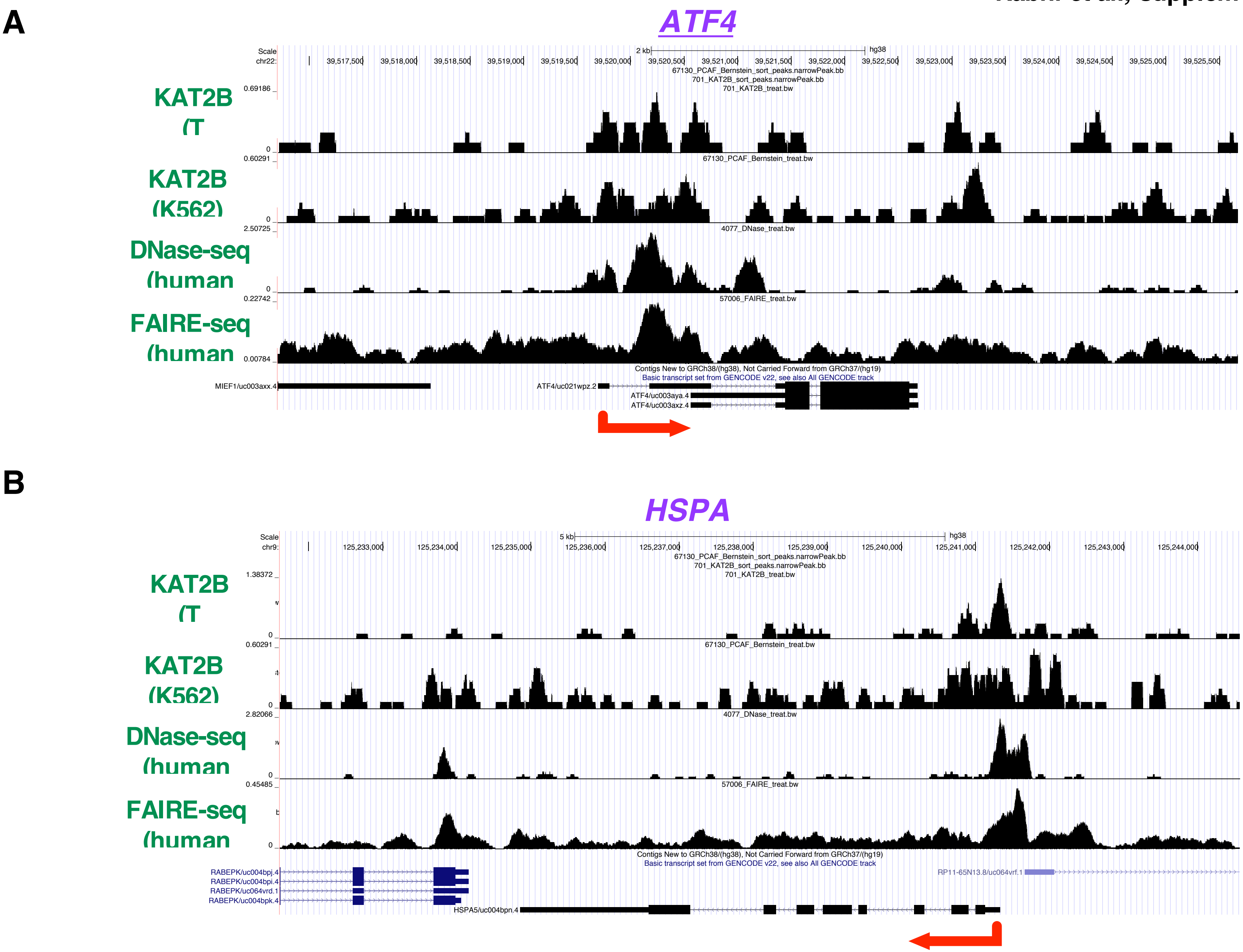

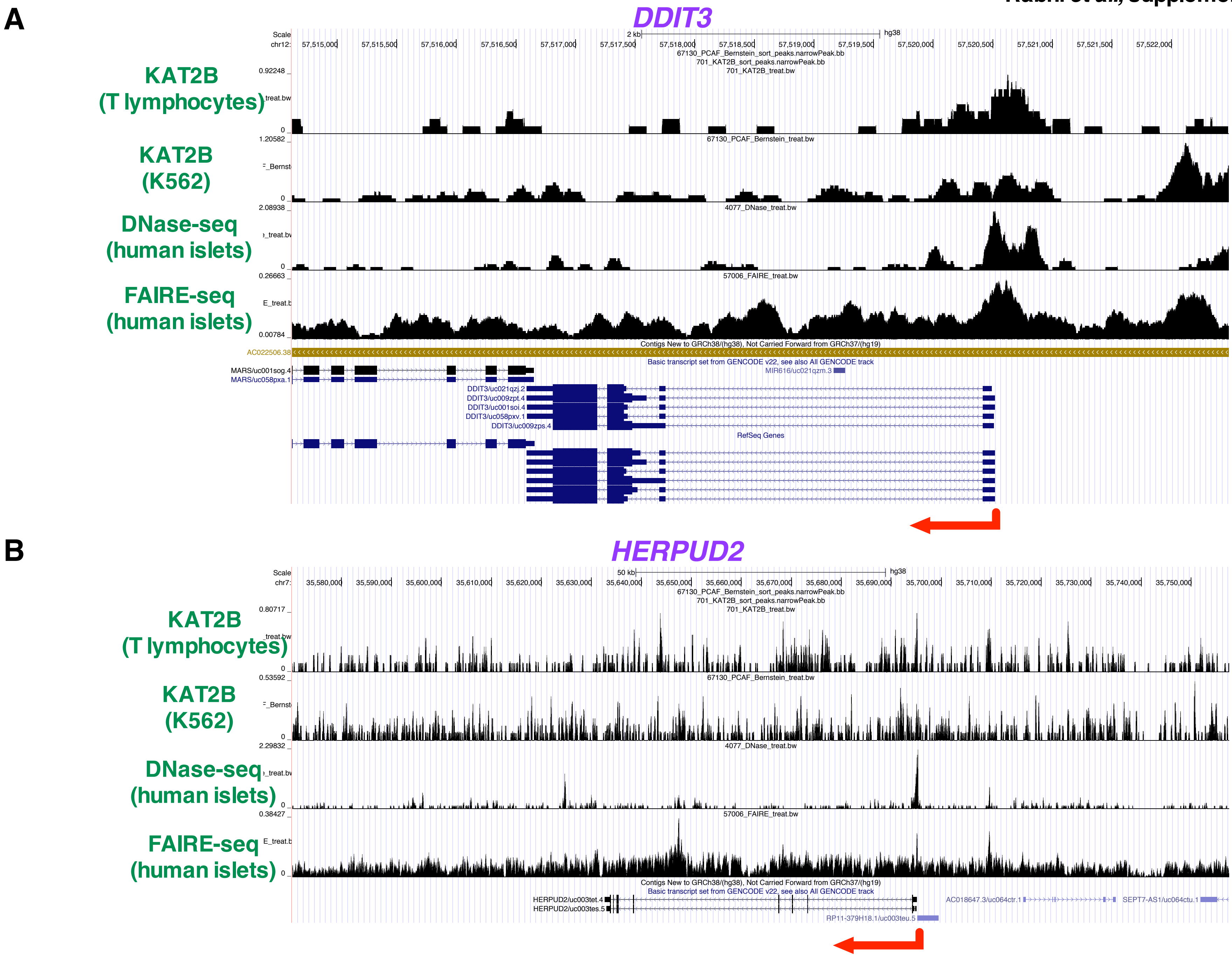
A
DDIT3
KAT2B
(T lymphocytes)
KAT2B
(K562)
DNase-seq
(human islets)
FAIRE-seq
(human islets)
B
HERPUD2
KAT2B
(T lymphocytes)
KAT2B
(K562)
DNase-seq
(human islets)
FAIRE-seq
(human islets)

Supplementary Table 3 : List of Kat2b target genes involved in UPRer obtained after functional enrichment analysis of ChIP-seq data using g:profiler.

# gene	chrom	start	stop	peak	score
Aars	8	113534882	113534984	MACS_peak_72058	72.56
Amfr	8	96492296	96492414	MACS_peak_71535	54.75
Atf3	1	192944961	192945042	MACS_peak_5658	53.07
Atf4	15	80072002	80072475	MACS_peak_27438	199.26
Atf6	1	172624501	172624613	MACS_peak_5039	64.60
Atf6b	17	34754982	34755120	MACS_peak_32030	77.82
Bak1	17	27140646	27140753	MACS_peak_31797	60.11
Bax	7	52728577	52728678	MACS_peak_65634	53.10
Bfar	16	13674200	13674306	MACS_peak_28485	75.80
Casp12	9	5352861	5352977	MACS_peak_72799	62.92
Ccnd1	7	152155992	152156145	MACS_peak_68634	95.86
Creb3l1	2	91795098	91795259	MACS_peak_40857	92.27
Creb3l2	6	37279477	37279597	MACS_peak_59686	61.30
Creb3l3	10	80559047	80559159	MACS_peak_8071	51.11
CREBRF	17	26832471	26832579	MACS_peak_31789	50.41
Ddit3	10	126765143	126765253	MACS_peak_9462	58.62
Derl1	15	57703000	57703136	MACS_peak_26820	67.12
Derl3	10	75348714	75348822	MACS_peak_7923	66.35
Dnajc3	14	119330505	119330625	MACS_peak_25075	53.61
Eif2ak2	17	79241906	79242036	MACS_peak_33369	65.19
Eif2ak3	6	70788465	70788566	MACS_peak_60750	62.15
Eif2ak4	2	118207375	118207516	MACS_peak_41592	76.56
Ep300	15	81411924	81412048	MACS_peak_27475	59.75
Ern1	11	106263714	106263823	MACS_peak_12615	50.04
Ern2	7	129314808	129314913	MACS_peak_67968	51.54
Ero1l	14	45891706	45891828	MACS_peak_22925	52.90
H47	7	73229273	73229375	MACS_peak_66337	60.75
Herpud1	8	96909128	96909233	MACS_peak_71542	67.72
Hspa5	2	34580993	34581117	MACS_peak_39197	59.75
Ifng	10	117864304	117864403	MACS_peak_9200	67.84
Nck1	9	100388513	100388623	MACS_peak_75579	51.93
Nck2	1	43477679	43477785	MACS_peak_1163	51.16
Nfe2l2	2	75521714	75521834	MACS_peak_40367	61.30
Nkx3-1	14	69803685	69803819	MACS_peak_23665	98.25
Parp16	9	65089706	65089829	MACS_peak_74573	52.55
Ppp1r15a	7	52777778	52777971	MACS_peak_65637	88.62
Ptpn1	2	167740396	167740499	MACS_peak_43023	52.31
Ptpn2	18	67866477	67866585	MACS_peak_35678	58.21
Rnf121	7	109146055	109146137	MACS_peak_67367	60.65
Serp1	3	58328397	58328520	MACS_peak_45138	60.13
Stc2	11	31247176	31247294	MACS_peak_10457	62.10
Stub1	17	25935067	25935178	MACS_peak_31753	54.75
Vapb	2	173578373	173578492	MACS_peak_43203	58.77
Xbp1	11	5448837	5448890	MACS_peak_9641	58.92
Yod1	1	132602734	132602850	MACS_peak_3889	62.92

Supplementary Table 4 : Donor informations

	Age	BMI	HBa1c
Control islet	46	19	5.6
Control islet	51	21.8	N.D.
Control islet	46	19	6.2
Control islet	48	21	5.9
Diabetic islet	59	37.7	7
Diabetic islet	56	40.1	9.5
Diabetic islet	62	32.7	7.5
Diabetic islet	58	32.9	7.2

Supplementary Table 5 : List of data sets used in bioinformatical analyses.

Data set type	Data set ID	URL link	reference
human islet expression	GSE38642	http://www.ncbi.nlm.nih.gov/sites/GDSbrowser?acc=GDS433	Taneera J, et al. Cell Metab 2012 Jul 3;16(1):122-34. PMID: 227688
human islet expression	GSE20966	http://www.ncbi.nlm.nih.gov/sites/GDSbrowser?acc=GDS378	Marselli L, et al. PLoS One 2010 Jul 13;5(7):e11499. PMID: 206446
human ChIP-seq	GSM393947	http://www.ncbi.nlm.nih.gov/geo/query/acc.cgi?acc=GSM393	Wang Z, et al. Cell 2009 PMID: 19698979
human ChIP-seq	GSM831007	http://www.ncbi.nlm.nih.gov/geo/query/acc.cgi?acc=GSM831	Ram O, et al. Cell 2011 PMID: 22196736
human ChIP-seq	GSM586891	http://www.ncbi.nlm.nih.gov/geo/query/acc.cgi?acc=GSM586	Stitzel ML, et al. Cell Metab. 2010 PMID: 21035756
human ChIP-seq	GSM1026917	http://www.ncbi.nlm.nih.gov/geo/query/acc.cgi?acc=GSM102	Paul DS, et al. Genome Res. 2013 PMID: 23570689

Supplementary Table 6 : List of oligonucleotides used in qRT-PCR and ChIP-qPCR analyses.

Gene name	Gene symbol	Species	Primer
lysine acetyltransferase 2B	*Kat2b*	mouse	GGCGTGTACTCCGCCTGCAA
			AGGGCATGGCTACAGCTTCGAC
Insulin1	*Ins1*	mouse	GCCAAACAGCAAAGTCCAGG
			GTTGAAACAATGACCTGCTTGC
Insulin2	*Ins2*	mouse	CAGCAAGCAGGAAGCCTATCT
			CAGGTGGGAACCACAAAGGT
Pancreatic and duodenal homeobox 1	*Pdx1*	*mouse*	ATTGTGCGGTGACCTCGGGC
			GATGCTGGAGGGCTGTGGCG
v-maf musculoaponeurotic fibrosarcoma oncogene family, protein A (avian)	*Mafa*	mouse	TCCGACTGAAACAGAAGCGG
			CTCTGGAGCTGGCACTTCTC
proprotein convertase subtilisin/kexin type 1	*Pcsk1*	mouse	TGATGATCGTGTGACGTGGG
			GGCAGAGCTGCAGTCATTCT
proprotein convertase subtilisin/kexin type 1	*Pcsk2*	mouse	AAAGATGGCGCTGCAACAAG
			TTGCCCAGTGTTGAACAGGT
carboxypeptidase E	*Cpe*	*mouse*	AAACTTACAGCCTCCGCTCC
			CAAGCTCAAAGTCCACCCCA
solute carrier family 30 (zinc transporter), member 8	*Slc30a8*	mouse	GGCTATCCTCACTGATGCGG
			ACCGAGGATCTCTGCTCGATA
potassium channel, inwardly rectifying subfamily J, member 11	*Kcnj11*	mouse	CACAAGCTGGGTTGGGGGCTC
			TGCCCCTCAGCTGGGTTCTGC
ATP-binding cassette, sub-family C (CFTR/MRP), member 8	*Abcc8*	mouse	TGTCATCCGGGTGCGGAGGT
			GAAAGCGCACCCCCAGGTCC
chromogranin A	*ChgA*	*mouse*	CGGGCAAGTTTTTGCCCTTC
			TGACTTCCAGGACGCACTTC
islet amyloid polypeptide	*Iapp*	mouse	GATATTGCTGCCTCGGACCA
			GGGTTGCTACCACTTCTGACA
protein tyrosine phosphatase, receptor type, N	*Ptprn*	mouse	AAGGTTCCGGTGATGGACAC
			ACGTGAAACCTGTACGGGAG
activating transcription factor 6	*Atf6*	mouse	CATGTGGTGAATGTGCTGCC
			CACAGCGATATCCGAACCCA
DNA-damage-inducible transcript 3	*Ddit3*	mouse	CTGCCTTTCACCTTGGAGAC
			CGTTTCCTGGGGATGAGATA
tein phosphatase 1, regulatory (inhibitor) subunit	*Ppp1r15a*	mouse	GAGATTCCTCTAAAAGCTCGG
			CAGGGACCTCGACGGCAGC
heat shock 70kDa protein 5 (glucose-regulated protein, 78kDa)	*Hspa5*	*mouse*	CATGGTTCTCACTAAAATGAAAGG
			GCTGGTACAGTAACAACTG
heat shock protein 90kDa beta (Grp94), member 1	*Hsp90b1*	mouse	AATAGAAAGAATGCTTCGCC
			TCTTCAGGCTCTTCTTCTGG
activating transcription factor 4	*Atf4*	mouse	ATGGCCGGCTATGGATGAT
			CGAAGTCAAACTCTTTCAGATCCATT
DnaJ (Hsp40) homolog, subfamily C, member 3	*Dnajc3*	mouse	TCCTGGTGGACCTGCAGTACG
			CTGCGAGTAATTTCTTCCCC
X-box binding protein 1 spliced	*Xbp1s*	*mouse*	GAGTCCGCAGCAGGTG
			GTGTCAGAGTCCATGGGA
X-box binding protein 1	*Xbp1t*	mouse	GAGCAGCAAGTGGTGGATTT
			CCGTGAGTTTTCTCCCGTAA
ER degradation enhancer, mannosidase alpha-like 1	*Edem1*	mouse	AAGTCTCAGGAGCTCAGAGTCATTAA
			CGATCTGGCGCATGTAGATG
endoplasmic reticulum oxidoreductase beta	*Ero1b*	mouse	GGGCCAAGTCATTAAAGGAA
			TTTATCGCACCCAACACAGT
protein disulfide isomerase family A, member 4	*Pdia4*	*mouse*	AGTCAAGGTGGTGGTGGGAAAG
			TGGGAGCAAAATAGATGGTAGGG
Lysine acetyltransferase 2B	*KAT2B*	human	GGTGAAGAGCCATCAAAGCG
			GACTCGCTGTAAGTCTGCCA
Insulin	*hIns*	human	AGCCTTTGTGAACCAACACC
			GCTGGTAGAGGGAGCAGATG
Glucagon	*hGlucagon*	human	CATTCACAGGGCACATTCAC
			CGGCCAAGTTCTTCAACAAT
Somatostatine	*hSST*	human	AGCTGCTGTCTGAACCCAAC
			CCATAGCCG GGTTTGAGTTA

Activating transcription factor 6	*hATF6*	human	AGCAGCACCCAAGACTCAAAC GCATAAGCGTTGGTACTGTCTGA
X-box binding protein 1 spliced	*hXBP1t*	human	CCGCAGCAGGTGCAGG GGGGCTTGGTATATATGTGG
X-box binding protein 1	*hXBP-1s*	human	CCTTGTAGTTGAGAACCAGG GGGGCTTGGTATATATGTGG
CHIP_qPCR	*Atf6 promoter*	mouse	CCCATGGCTTGACATCTGCT GACCTCGTTCTCTGGAAGGC